Journal of Controlled Release 386 (2025) 114134

Contents lists available at ScienceDirect

Journal of Controlled Release

journal homepage: www.elsevier.com/locate/jconrel

The role of PEGylation in the pulmonary delivery of antifibrotic liposomal therapies

Marina Piñol-Cancer [a,b,g], Laura Fernández-Méndez [a,b], Juliana Carrillo-Romero [a,c], Ainhize Urkola-Arsuaga [a], Mikel Azkargorta [d], Félix Elortza [d], Felipe Goñi-de-Cerio [c], Cristina García-Mouton [e,f], Claudia Miranda-Pérez de Alejo [a,b], Ermal Ismalaj [a], Olga Cañadas [e,f], Jesús Pérez-Gil [e,f], Jesús Ruíz-Cabello [a,g,h,i,*], Susana Carregal-Romero [a,g,h,*]

[a] Center for Cooperative Research in Biomaterials (CIC biomaGUNE), Basque Research and Technology Alliance (BRTA), 20014 Donostia, Spain
[b] Euskal Herriko Unibertsitatea (UPV/ EHU), 20018 Donostia, Spain
[c] GAIKER Technology Centre, Basque Research and Technology Alliance (BRTA), 48170 Zamudio, Spain
[d] Proteomics Platform CIC bioGUNE, Basque Research and Technology Alliance (BRTA), CIBERehd, Bizkaia Science and Technology Park, 48160 Derio, Spain
[e] Departamento de Bioquímica y Biología Molecular, Facultad de Ciencias Biológicas, Universidad Complutense de Madrid, 28040 Madrid, Spain
[f] Instituto de Investigación Hospital 12 de Octubre (imas12), 28041 Madrid, Spain
[g] CIBER of Respiratory Diseases (CIBERES), 28029 Madrid, Spain
[h] Ikerbasque, Basque Foundation for Science, 48013 Bilbao, Spain
[i] Department of Chemistry in Pharmaceutical Sciences, Complutense University of Madrid, 28040 Madrid, Spain

ARTICLE INFO

Keywords:
PEGylation
Lipid nanoparticles
Mucus interaction
Lung surfactant corona
Pulmonary fibrosis
Pirfenidone

ABSTRACT

PEGylation is commonly used to improve the pharmacokinetics and efficacy of intravenously administered drug nanocarriers; however its impact on pulmonary drug delivery remains unclear. While previous studies have focused on its role in crossing the lung mucosal barrier and stabilizing formulations for nebulization, less is known about its effects on lung surfactant corona composition, biodistribution, and therapeutic efficacy. Here, we present a multiscale study on how PEG-free and PEGylated liposomes loaded with pirfenidone interact with pulmonary barriers. PEGylation increased mucus penetration and reduced protein adsorption in the lung surfactant corona. However, statistical analysis of functional proteins showed only moderate changes in anti-inflammatory and adhesion proteins, with no apparent effect on key surfactant proteins that influence liposome fate in the lung. This correlated with similar biodistributions and retention times in both healthy and fibrotic lungs for PEG-free and PEGylated liposomes. Concerningly, PEGylated liposomes enhanced native surfactant fluidity, potentially altering lung function. In a bleomycin-induced pulmonary fibrosis model, both PEG-free and PEGylated liposomes improved the antifibrotic efficacy of pirfenidone. However, PEGylation attenuated the reduction in fibrotic biomarkers within the lung fluid. These findings suggest that, although PEGylation facilitates mucus penetration, it does not significantly enhance therapeutic outcomes and may adversely affect lung function. This study provides critical insights into the optimization of lipid-based nanocarriers for pulmonary fibrosis and other lung diseases.

1. Introduction

Pulmonary fibrosis (PF) is a progressive and fatal respiratory disease characterized by lung scarring and respiratory impairment, with a median survival of 2–5 years. [1] This age-associated disease has a global prevalence ranging from 7 to 1650 per 100,000 persons and is a significant long-term complication of COVID-19, even in asymptomatic individuals. [2–4] As a result, public health experts consider PF a global threat. [3,5] Despite advances in understanding its molecular basis, treatment remains limited. Patients rely on orally administered drugs that alleviate symptoms but do not halt disease progression and often cause severe side effects. [6] Thus, advanced antifibrotic strategies are

* Corresponding authors at: Center for Cooperative Research in Biomaterials (CIC biomaGUNE), Basque Research and Technology Alliance (BRTA), 20014 Donostia, Spain.
E-mail addresses: jruizcabello@cicbiomagune.es (J. Ruíz-Cabello), scarregal@cicbiomagune.es (S. Carregal-Romero).

https://doi.org/10.1016/j.jconrel.2025.114134
Received 6 May 2025; Received in revised form 28 July 2025; Accepted 14 August 2025
Available online 18 August 2025

needed to improve patients' quality of life and potentially offer a cure.

Pulmonary administered nanoparticle-based drug delivery systems are promising for treating pulmonary fibrosis. [7] The inhalation route provides a noninvasive method to target fibrotic lesions in distal lung areas, ensuring fast absorption, high delivery efficiency, and low therapeutic doses. [8] Lung administration bypasses the mononuclear phagocyte system, which clears most intravenously (i.v.) administered nanomedicines. [9–11] Encapsulation of antifibrotic drugs in nanocarriers enables controlled drug release, increased stability, and targeted delivery to fibrotic lesions. [12] However, biological barriers such as rapid clearance, potential toxicity, and ineffective particle deposition necessitate understanding nano-bio interactions to optimize nanoparticle (NP) design. [13–15]

Mucociliary clearance (MCC) is the first defense mechanism against inhaled antifibrotic NPs. In PF, MCC undergoes morphological changes, including mucus hypersecretion and plug formation. [16] Pulmonary mucus, a hydrogel composed of 95 % water and 5 % proteins, salts, lipids, DNA, and debris, has a net negative charge and variable pore size (~500 nm). To avoid entrapment, between other physicochemical properties, nanoparticles (NPs) should be smaller than the mucus pore size and carry a neutral or negative charge to minimize electrostatic or hydrophobic interactions. [17]

Another key interaction is the formation of the lung surfactant (LS) corona. [13,18,19] LS, a lipid-protein mixture secreted by epithelial cells, reduces surface tension and supports immune functions. Surfactant proteins (SP-A, SP-B, SP-C, and SP-D) play essential roles in lung biophysics and immunity. Similar to i.v. NP-protein coronas, exposure of NPs to deep lung tissue leads to LS corona formation through surface adsorption. [20] NP surface properties influence the LS corona composition, affecting translocation, [21] retention time, [22] immune response, cytotoxicity, [23] stability, cellular uptake, [13] and drug release.

PEGylation, the covalent attachment of polyethylene glycol (PEG) chains to NPs, is widely used in i.v. nanomedicines to reduce protein corona formation, enhance circulation time, reduce immunogenicity, and improve biocompatibility. [11,24,25] However, concerns have emerged regarding PEG-induced immunogenicity and allergic reactions, [26,27] particularly due to rising PEG-specific antibodies in patients treated with mRNA SARS-CoV-2 vaccines. [28] In pulmonary nanomedicine, the effects of PEGylation remain unclear, and inhalable PEGylated nanomedicines are rare in clinics. [29] While PEGylation has been reported to stabilize aerosol formulations, enhance mucus penetration, reduce clearance, improve stability, prolong lung residence, and mitigate cytotoxicity, [30] studies also indicate reduced cellular uptake, potential accumulation, and immunogenicity risks, leading to possible pulmonary toxicity. [31] The variation in lung diseases and their unique regional characteristics further underpins the need to assess whether PEGylation optimizes nano-bio interactions for pulmonary antifibrotic therapies.

This study examines the role of PEGylation on antifibrotic pirfenidone-loaded liposomes regarding their interaction with lung mucus, lung surfactant, alveolar cells and lung tissue *in vivo* both in healthy and fibrotic animal models. Specifically, we assessed NP-mucus penetration, LS corona proteomics, LS functional stability, NP retention and biodistribution, and the antifibrotic effects of both PEGylated and non-PEGylated LPs. While PEGylation reduced LS corona formation, modified the protein composition and enhanced mucus penetration, it led to concerning interactions with native LS and had slight effects and no significant improvements on drug stability, biodistribution, lung retention, and antifibrotic efficacy. These findings question the necessity of PEGylation for pulmonary antifibrotic NP administration and provide critical insights into the development of safer and more effective nanomedicines for pulmonary fibrosis that could be extended to other inhalable nanomedicines.

2. Materials and methods

2.1. Synthesis and characterization of LP and LP-PEG

Liposomes were synthesized by the thin film hydration method followed by membrane extrusion. [32] For LP synthesis with PFD, 27 μmol of DPPC, 3 μmol of *lyso*-PC (90:10 of DPPC:lyso-PC)) and 22 μmol of PFD were dissolved with 5 mL of $CHCl_3$: CH_3OH (6:1) in a round bottom flask. For LP-PEG synthesis with PFD, 25.8 μmol of DPPC, 3 μmol of *lyso*-PC, 1.2 μmol of DSPE-PEG (86:10:4 of DPPC:lyso-PC:DSPE-PEG) and 27 μmol of PFD were mixed in the same solvent mixture. Rotary evaporation under reduced pressure was used to form the phospholipid film. The film was then hydrated with 5 mL of HPLC water and extruded (with 400, 200, and 100 nm membranes) to obtain the desired size of 100 nm. To synthesize IONP-loaded LP and LP-PEG, IONPs were synthesized as previously described. [33] For 5 μmol of lipids, 1 mL of IONP ([Fe] = 1 mg/mL) was added in the hydration step followed by 10 freeze-thaw cycles prior to extrusion. Free PFD or IONP were separated from the liposomes by filtration and centrifugation. The encapsulation of PFD was analyzed by UV–vis spectrophotometry at 317 nm after disruption of the liposomes with methanol for 15 min. [34] The phospholipid content was measured by the Rouser method. [35] The molar ratios of phospholipid:PFD were 3:1 and 4:1 for LP and LP-PEG, respectively. The encapsulation efficiency, determined by UV–Vis spectroscopy after liposome disruption in a MeOH:H_2O mixture, was 45 % for LP and 27 % for LP-PEG. Loading capacity, calculated as the amount of encapsulated PFD relative to the total lipid weight (loading capacity = mass of loaded PFD / total lipid mass × 100 %), was 8.9 % for LP and 6.6 % for LP-PEG. The iron content in IONP-loaded liposomes was determined by ICP-MS (Thermo Fisher iCap-Q). The liposome hydrodynamic diameter and zeta-potential were measured using a Zetasizer NanoZS (Malvern) and the morphology was analyzed by CryoTEM using a JEOL JEM 2100F microscope operating at 80 kV and equipped using a GATAN Model 626 cryo-transfer sample holder. FT-IR experiments were conducted with a Bruker Invenio-X spectrophotometer. To calculate the surface density of PEG (2 kDa) chains, we assume a bilayer thickness of 5 nm and a surface area of the head group if 0.61 nm^2 based on previous publications, [36,37] and followed the method of Xu et al. [38]

2.2. Mucus penetration assay

A surrogate for pulmonary mucus was synthesized according to the protocol developed by Huck et al. [39] Briefly, 50 mg of NaCl, 22 mg of KCl, 50 mg porcine stomach mucin type II, 18.1 mg of Tris ≥99.8 % (Bio-Rad), 50 mg of deoxyribonucleic acid, and 100 μL 0.15 M diethylenetriamine pentaacetic acid were added to 8 mL of ultrapure water. The solution was mixed with continuous agitation at 800 rpm for 24 h. Then, 50 mg of OmniPur® Casamino Acids (Calbiochem®) and 90 mg of poly (acrylic)acid (Carbopol 974P NF) were added. The solution was stirred again for 24 h. The pH was then adjusted to 7.0 by adding Tris 1 M. Finally, 50 μL of egg yolk emulsion was added to the mixture to mimic the biochemical and the physical properties of natural pulmonary mucus, [40,41] and the final volume was adjusted to 10 mL with ultrapure water. To determine the penetration capacity of LP and LP-PEG, 100 μL of pulmonary mucus surrogate was placed in the donor chamber of Transwell® polycarbonate inserts (0.4 μm pore size and 0.33 cm^2 surface area) and the acceptor chambers were filled with 200 μL of PBS 1×. The inserts were incubated at 37 °C with continuous agitation on a shaker at 200 rpm for 10 min. Then, 50 μL of either LP or LP-PEG (1 mg/mL) was added to the mucus layer, and the plate was kept at 37 °C. Apical and basolateral samples were collected at different time points (1, 2, 4, 6, 16, and 24 h) to measure the corresponding fluorescence intensity (λ_{exc}/ λ_{em}: 480/510 nm). Transwell inserts containing mucus but no liposomes were used as a negative control.

2.3. Analysis of protein corona formation with native lung surfactant

The analysis of the lung surfactant corona was performed according to the protocol developed by Raesch et al. [20] Porcine LS was isolated as previously described, [42] and diluted in Tris-buffered saline (TBS) containing 150 mM NaCl, and 5 mM Tris at pH 7.4. It was then mixed with the LPs at a ratio of 9:1 (μg of IONP loaded liposomes per μg of protein in LS). The mixture was incubated at 37 °C with continuous shaking at 400 rpm to avoid surfactant precipitation. After 1 h, the LPs were magnetically separated, and the supernatant was discarded. To ensure complete washing, the precipitate was subjected to three cycles of re-dispersion in 1.5 mL TBS, followed by magnetic separation. Total protein content was quantified using a BCA assay kit. For proteomic analysis, samples were stored at −80 °C until protein corona analysis was performed using mass spectrometry (more information in the SI).

2.4. Cellular uptake

HLF were seeded in 24-well plates and allowed to adhere overnight. The cells were treated with serum-free medium containing 5 ng/mL TGF-β1 to induce myofibroblast differentiation. After 24 h, 50 μM LP or LP-PEG were added to the serum-free medium. THP1 cells were seeded with 100 ng/mL PMA, and after 24 h, the medium was changed to add 20 ng/mL IL-4 and IL-13 for 48 h to stimulate the M2 phenotype. Then, the cells were incubated for 24 h with 50 μM of LP or LP-PEG. A549 cells were similarly seeded overnight, followed by treatment with 50 μM LP or LP-PEG fluorescently labeled with $DiOC_{18}$ (484/521 nm) in complete DMEM. To investigate the influence of LS corona formation, LP and LP-PEG were incubated with LS at a 9:1 ratio (μg lipids:μg protein) for 5 min at 37 °C before being added to both cell types. Following 24 h of incubation, cells were washed with PBS, trypsinized, and analyzed for cellular uptake *via* MACSQuant10 flow cytometry.

2.5. Effect of PEGylation of nanoparticles on surfactant function

We used a captive bubble surfactometer (CBS) to evaluate the effect of nanoparticle PEGylation on the interfacial properties of LS. This device somehow mimics respiratory mechanics at the alveolar air-liquid interface by monitoring the change in shape of a millimetric air bubble in an experimental chamber filled with an aqueous solution (5 mM Tris-HCl pH 7.4 buffer with 150 mM NaCl and 10 % (*w*/w) sucrose), thermostated at 37 °C, and subjected to compression-expansion cycling at physiological rates. [43] To study surfactant adsorption to a clean air/liquid interface, 3 μg of LS, alone or mixed with 10 % (w/w) LP or LP-PEG, was injected underneath the air bubble. Then, the chamber was sealed, and the bubble was expanded for 5 min to characterize the respreading ability of LS. Next, the air bubble was subjected to subsequent quasi-static and dynamic compression/expansion cycles to analyze the reorganization of the interfacial film and its ability to reduce surface tension to very low values upon compression. [44]

2.6. Determination of the release profile of LPs with lung surfactant

To study the *in vitro* release of PFD from LP and LP-PEG, its release was measured at different time points using UV–vis spectroscopy at 314 nm. MINI dialyzers with a molecular weight of 3.5 KDa (Slide-A-Lyzer™ MINI) were used to dialyze 100 μL of LP or LP-PEG with 1 mL of PBS at pH 7.4. To further investigate the effect of the lung surfactant corona on PFD release, liposomes were mixed with the lung surfactant at a phospholipid: protein ratio of 20:1.

Immunofluorescence assays. Treatment sequences and time points were selected based on the temporal expression patterns of fibrosis-related biomarkers and prior optimization studies. HLF were seeded on coverslips in 24-well plates and allowed to settle in complete medium at 37 °C with 5 % CO_2 overnight. For α-SMA expression analysis, cells were treated with 30 μg/mL of free PFD or PFD encapsulated in LP or LP-PEG for 4 h, [7] followed by incubation with serum-free medium containing 10 ng/mL TGF-β1 for 48 h. For control experiments involving activated cells not treated with antifibrotic LP or LP-PEG, an equivalent volume of sterile water was used as a vehicle control. The volume of water added was kept low to avoid affecting osmolarity or pH, and no signs of cell stress or membrane disruption were observed. All groups were handled identically in terms of timing, volume, and mixing to ensure consistency across conditions. For COL1A1 expression analysis, cells were incubated for 48 h with the same treatments in the presence of 10 ng/mL TGF-β1 in serum-free medium following previous drug screening protocols. [45] After TGF-β1 stimulation, the cells in both experiments were fixed with 4 % paraformaldehyde (PFA) and permeabilized using 0.1 % Triton X-100. Cells were blocked with 1 % bovine serum albumin (BSA) and 5 % goat serum and then incubated with primary antibodies against α-SMA and COL1A1. Secondary antibodies conjugated to Alexa Fluor 555 and Alexa Fluor 488 were used for detection, respectively. Cell nuclei were stained with DAPI, and images were captured using a Zeiss Cell Observer Axio Observer. The mean fluorescence intensities of α-SMA and COL1A1 were quantified using Image J software. For immunofluorescence staining of Ki67, HLF were seeded under similar conditions. The next day, serum-free medium with 5 ng/mL TGF-β1 was added for 24 h, followed by a 4-h treatment with 30 μg/mL of PFD (encapsulated in LP, LP-PEG, or unencapsulated). [46] After treatment, the medium was replaced with serum-free medium for 24 h. The cells were then washed with PBS, fixed with 4 % PFA, and blocked with 3 % BSA. Primary antibody against Ki67 was applied, followed by detection using an Alexa Fluor 488-conjugated secondary antibody. Quantification of Ki67-positive cells was conducted using Image J software.

2.7. Wound-healing assay

HLF were seeded overnight in a 24-well plate, and the next day, the medium was changed to serum-free medium containing 2 ng/mL TGF-β. After 24 h, the cells were scraped mechanically with a sterile tip and washed twice with serum-free medium. The cells were then incubated with 30 μg/mL PFD and the same amount of PFD encapsulated in LP or LP-PEG in serum-free medium for 4 h, followed by incubation with serum-free medium for 24 h. Migration images were captured with a Leica DM IL LED inverted microscope before and after 24 h of scratching to determine the percentage of wound healing. Quantification was performed using Image J software.

2.8. Ethical considerations

All animal experiments were performed in accordance with the Spanish animal protection policy (RD53/2013), which complies with the requirements of the European Union Directive 2010/63/ EU, in the CIC biomaGUNE animal facility. Mice were acclimatized for a minimum period of one week before starting any experiment. They were always anesthetized by inhalation with isoflurane (3–5 %, Zoetis SL). Finally, the euthanasia method used was cervical dislocation to avoid damage to the lung tissue. The procedures were approved by the Ethics Committee of CIC biomaGUNE and authorized by the local authorities (Diputación Foral de Guipúzcoa: PRO-AES-SS-229 and PRO-AE-SS-323).

2.9. In vivo biodistribution study

Eight-week-old male C57BL/6 J mice were briefly anesthetized with inhaled isoflurane (3–5 %) and then IONP-loaded LP or LP-PEG were administered IT (0.1 mmol of Fe/kg mouse) to healthy C57BL/6 J mice. Magnetic resonance imaging (MRI) was performed 2, 72 and 144 h after IT administration. The experiments were performed using a Bruker Biospec 70/30 USR MRI 7 T system (Bruker Biospin GmbH, Ettlingen, Germany) connected to an AVANCE III console. Lung imaging was performed using a UTE3D sequence with respiratory gating to obtain

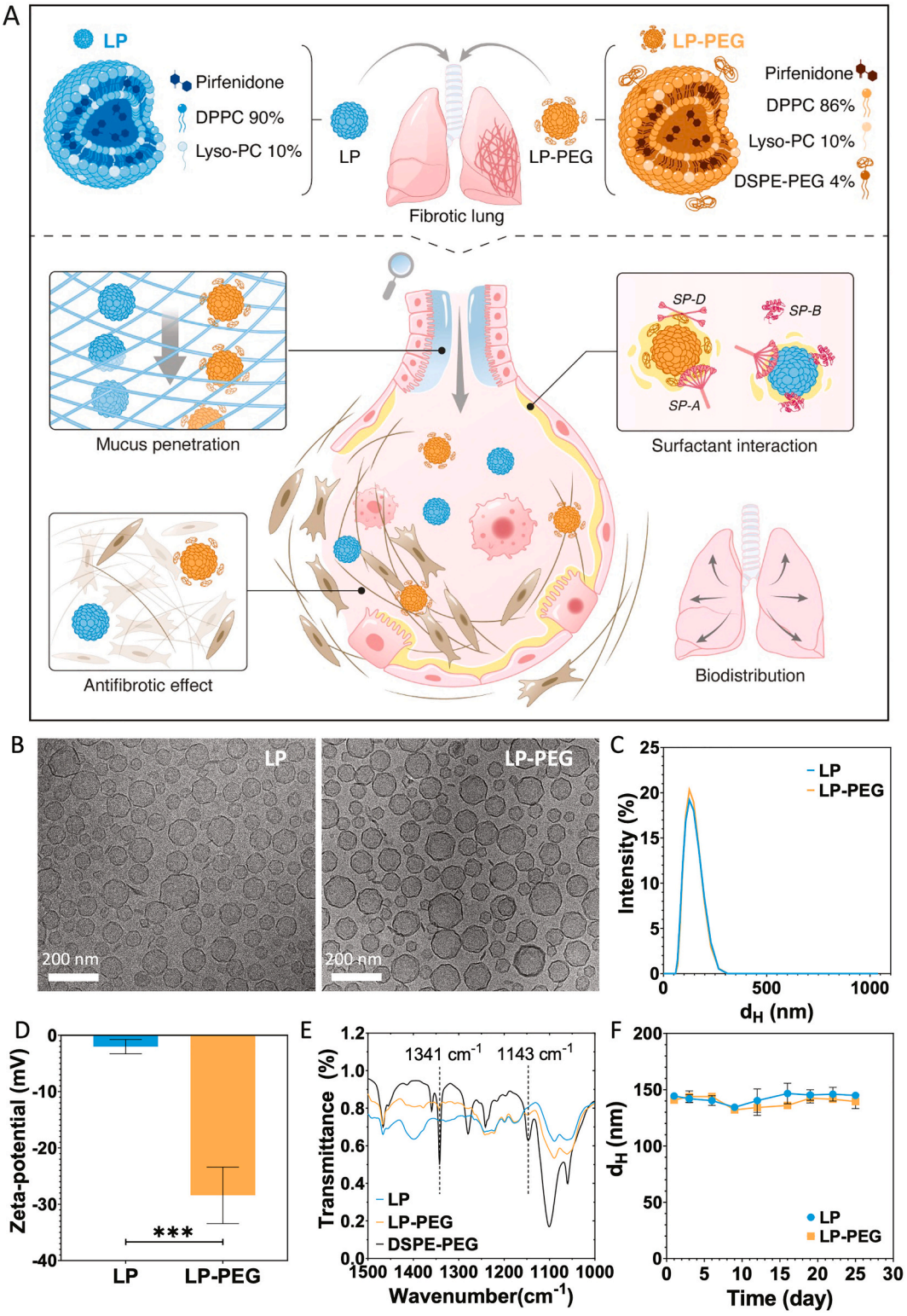

Fig. 1. Influence of PEGylation on pulmonary administered liposomes for pulmonary fibrosis. (A) Schematic representation of bare and PEGylated antifibrotic liposomes, their chemical composition, and their interactions with the lungs. (B) Cryo-TEM images of LP and LP-PEG. (C) Hydrodynamic diameters (d_H) of LP and LP-PEG and their corresponding zeta potential measurements (D) ($n = 3$, mean ± SD, Student's *t*-test ***$p < 0.001$). (E) FT-IR spectra highlighting the main peaks of DSPE-PEG present in LP-PEG and absent in LP. (F) Long-term colloidal stability of LP and LP-PEG in water (n = 3).

lung images and T_1 and T_2 maps of the liver. After 144 h, mice were euthanized, and organs were harvested and fixed in 4 % PFA for 48 h for histological analysis. To study biodistribution in mice with PF, PF was induced as described below. IONP-loaded liposomes were administered 10 days after BLEO IT. After 24 h, the lungs were processed for histological analysis. All analyses were performed using either ITK-snap or Image J software.

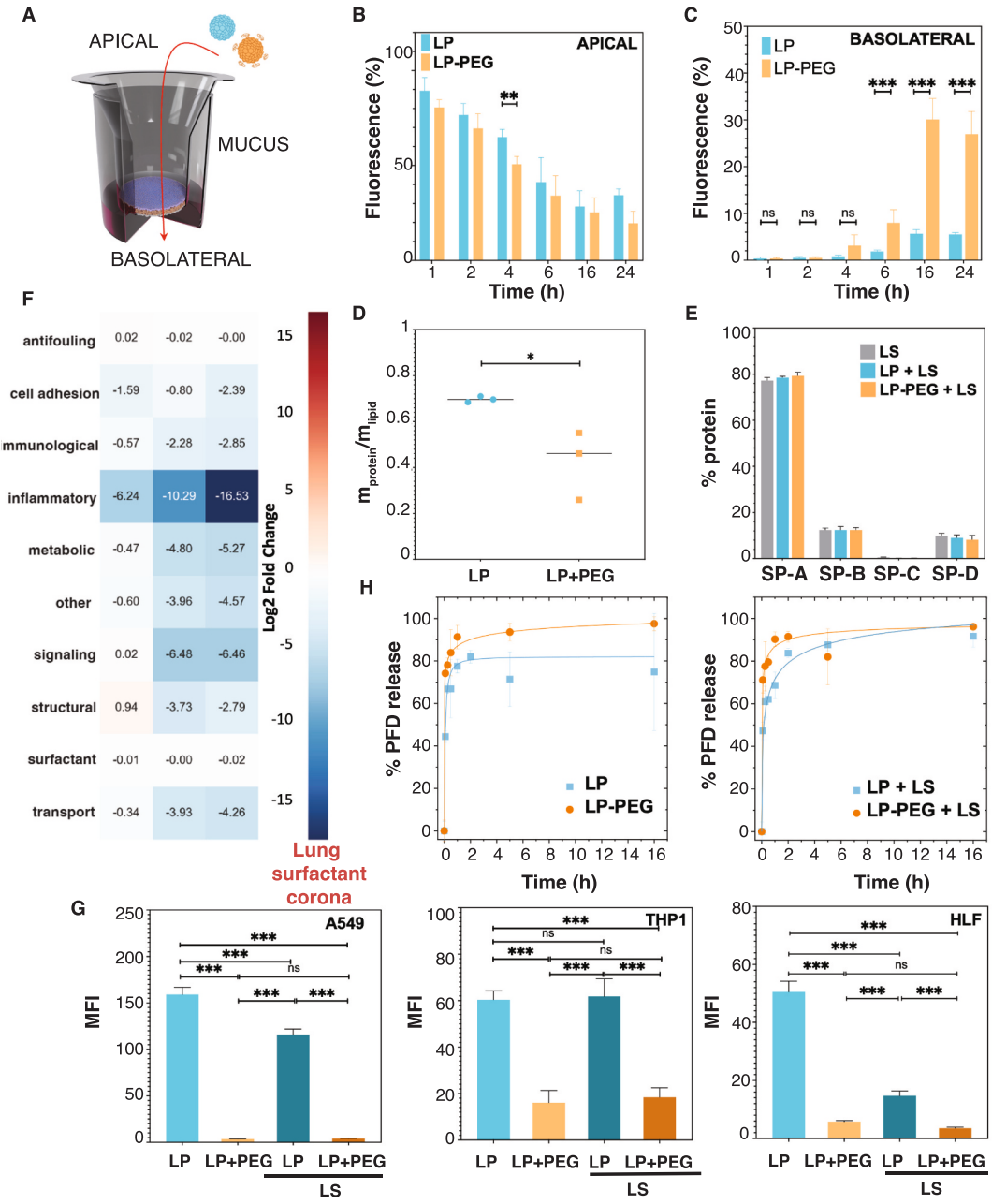

Fig. 2. Evaluation of the interaction of LP and LP-PEG with lung mucus and lung surfactant. (A) Schematic representation of the mucus penetration assay. Percentage (%) of fluorescent LP and LP-PEG in the apical (B) and basolateral (C) sides while crossing the mucus barrier ($n = 3$, mean ± SD, one-way ANOVA with Tukey's multiple comparison test: *$p < 0.05$, **$p < 0.01$, ***p < 0.01). (D) Total protein mass in the LS corona of LP and LP-PEG, normalized to the phospholipid mass in each LP (n = 3, mean ± SD, Student's *t*-test: *p < 0.05). (E) Percentage (%) of SPs relative to total protein mass. (F) Statistical comparison of the relative abundance of proteins grouped according to their biological function. (G) Flow cytometry results showing the mean fluorescence intensity (MFI) of fluorescently labeled LP and LP-PEG afte, r 24-h incubation uptaken by epithelial cells (A549), profibrotic macrophages (THP1), and human alveolar fibroblasts (HFL). Statistical analysis (n = 3; data represent mean ± SD) was performed using one-way ANOVA with Tukey's multiple comparison test (*p < 0.05, **p < 0.01, ***p < 0.01). (H) PFD release profiles of LP and LP-PEG without (left) and with LS corona (right).

2.10. Antifibrotic effect of PFD loaded LP and LP-PEG

Pulmonary fibrosis (PF) was induced in eight-week-old male C57BL/6NCrl mice *via* a single intratracheal instillation of 40 μL bleomycin (BLEO, 1.5 U/kg) in 0.9 % saline. Control mice received 40 μL of saline solution. The mice were monitored for lung injury using imaging techniques (PET/CT) and histological analysis for 10 days, followed by biodistribution and therapeutic studies. Animals were randomly assigned to four treatment groups: normal saline (NS), pirfenidone (PFD), liposomal PFD (LP), and PEGylated liposomal PFD (LP-PEG). Treatments (4.2 mg/kg PFD, free or liposome-loaded) were administered on days 10, 14, and 17, with NS as a control. *In vivo* computed tomography (CT) imaging was performed on days 0, 10, and 17, and analyzed using ITK-SNAP. Body weight was monitored throughout the study. On day 21, the mice were euthanized, and lung tissue and bronchoalveolar lavage (BAL) fluid were collected. The lungs were perfused with 4 % PFA for histology or harvested for hydroxyproline quantification using a commercial assay kit. BAL was processed by centrifugation, and the pellet was analyzed for inflammatory cells *via* flow cytometry (FACS) using fluorescence-conjugated antibodies (CD45, CD3, F4/80, Siglec F, and CD11c). The protein content of the supernatant was assessed with a BCA assay. Lung tissues were paraffin-

embedded for histological and immunofluorescence (IF) analyses. Three-micrometer serial sections were stained with hematoxylin and eosin (H&E), Masson's trichrome, picrosirius red, and IF markers for α-SMA and COL1A1. Biodistribution studies included Prussian blue and F4/80 immunohistochemistry (IHC), with staining performed using standard protocols. Inflammatory infiltration was quantified by nucleated cell counts in H&*E*-stained sections (40× magnification). Picrosirius red staining and IF signals for COL1A1 and α-SMA were quantified using ImageJ. Histological images were captured using an Axio Observer microscope (Zeiss).

2.11. Statistical analysis

All results were analyzed using GraphPad Prism software 8 or Origin 2020 and are expressed as mean ± SD. Statistical analyses were performed as indicated in the figure legends. One-way analysis of variance (ANOVA) with Tukey's multiple group test was used to analyze the differences between multiple groups. The Student's *t*-test was used to analyze the differences between the two groups. Differences were considered statistically significant when $^{*}p < 0.05$, $^{**}p < 0.01$ or $^{***}p < 0.001$.

3. Results and discussion

3.1. Synthesis of antifibrotic PEGylated liposomes

Lipid-based NPs, such as liposomes (LPs), are among the most promising drug nanocarriers for clinical applications. [47] They enable efficient encapsulation of both hydrophobic and hydrophilic drugs while offering high biocompatibility, biodegradability, improved drug stability, and enhanced delivery efficiency. [48] Given clinical relevance, we investigated how PEGylation influences liposome-lung interactions and the therapeutic efficacy of pirfenidone (PFD) using various biological models (Fig. 1A). Non-PEGylated (LP) and PEGylated (LP-PEG) liposomes were prepared *via* thin-film hydration and extrusion. [32] To optimize lung delivery, both formulations primarily consisted of dipalmitoyl phosphatidylcholine (DPPC), the main lung surfactant component, which is currently used in different inhalable nanomedicines for treating lung diseases. [49,50]

Small amounts of 1-palmitoyl-2-hydroxy-sn-glycero-3-phosphocholine (*lyso*-PC) were included in the lipid mixture to reduce bilayer permeability, [51] whereas 1,2-distearoyl-*sn*-glycero-3-phosphoethanolamine-N-methoxy(polyethylene glycol)-2000] (DSPE-PEG) was incorporated for PEGylation (Fig. 1A). *Lyso*-PC, a precursor in DPPC synthesis, also imparts thermosensitive properties to liposomes which could be used in future applications for stimuli-responsive drug delivery. [52]

The lipid composition was DPPC:*lyso*-PC (90:10 mol%) for LP, and DPPC:*lyso*-PC:DSPE-PEG (86:10:4 mol%) for LP-PEG. DSPE-PEG2000 was chosen for its good balance of reducing the protein corona formation without significantly reducing cell uptake. [27,53] Additionally, 4 % DSPE-PEG was selected because it is a moderate concentration that may help maintain colloidal stability. Smaller amounts may not provide sufficient steric stabilization, and larger amounts may promote the formation of non-liposomal structures, such as micelles or disks. [54] Both LP and LP-PEG compositions were inspired by similar lipid formulations that reached Phase II clinical trials (*e.g.*, ThermoDox), indicating prior safety validation in humans. [55] A 4 mol% content of DSPE-PEG2000 was incorporated into the liposomes using the post-insertion method to achieve surface PEGylation while maintaining the stability of the DPPC:*lyso-PC*-based drug-loaded liposomes. [56,57]

After extrusion and purification, the weight percentage of PEG incorporated into the liposomes was quantified using high-performance liquid chromatography (HPLC), yielding a value of 7.1 wt%. To evaluate the extent of surface shielding provided by PEG, we applied previously described methods to calculate the surface PEG density on liposomes. The analysis revealed a surface density of 11 PEG chains per 100 nm^2 for the 2KDa PEG, indicating that the PEG was likely arranged in a brush configuration. [38]

PFD encapsulation was achieved by mixing it with lipids before thin-film formation, as described previously, due to its limited aqueous solubility and high membrane permeability. [58,59] The final [phospholipid]:[PFD] ratio was 3:1 for LP and 4:1 for LP-PEG. Transmission electron cryomicroscopy (cryo-TEM) confirmed the formation of small unilamellar vesicles demonstrated by a single electronically dense outer layer (Fig. 1B) with LP and LP-PEG diameters of 78 and 81 nm, respectively (Fig. S1A). Dynamic light scattering (DLS) showed a hydrodynamic diameter (d_H) of 125 ± 2 nm for LP and 126 ± 2 nm for LP-PEG (Fig. 1C), along with a shift in zeta potential from −2 ± 1 mV for LP to −28 ± 5 mV for LP-PEG (Fig. 1D). This shift is likely due to the presence of DSPE-PEG in LP-PEG, which is negatively charged due to the ionization of its phosphate group in the DSPE moiety. Comparable d_H and zeta potential values were observed between the empty (Figs. S1B) and PFD-loaded LPs.

Fourier-transform infrared spectroscopy (FTIR) confirmed the distinct surface chemistries of LP and LP-PEG. In the spectra (Fig. 1E, S1C), DSPE-PEG presence was indicated by bands at 1144 and 1345 cm^{-1}, corresponding to C—O stretching (1143 cm^{-1}) and CH_2 wagging (1341 cm^{-1}). [60] Finally, colloidal stability was maintained for over 25 days at 4 °C (Fig. 1F). The polydispersity index values during this period, shown in Fig. S1D, indicated moderate polydispersity and a fair size distribution.

3.2. Nano-bio interactions of PEGylated LPs with lung barriers

The lung has non-cellular barriers that protect it against potentially toxic inhaled particles but also hinder nanomedicine delivery. [13,15] We examined LP and LP-PEG interactions with two key barriers: lung mucus and surfactant. The pulmonary mucus lines the respiratory tract, traps inhaled particles and prevents deep lung penetration. In PF, inflammation causes mucus accumulation in the alveoli. [16]

To assess the effect of PEGylation on mucus penetration, we used a mucin type II-based surrogate deposited on transwell inserts (Fig. 2A). [39] Fluorescently labeled LP or LP-PEG (with $DiOC_{18}$) were applied to the apical side and the fluorescence intensity was measured over time in both the apical and basolateral sides. The penetration of both liposomes into the mucus was similar, as the decrease in fluorescence in the apical part of the Transwell was comparable. However, LP-PEG diffused into the mucus more quickly, whilst LP remained retained, as the increase in fluorescence in the basolateral part was greater for LP-PEG than for LP (Fig. 2B,C). These results suggest that the enhanced basolateral signal observed for LP-PEG may be attributed to its improved penetration and diffusion across the mucus layer. This behavior likely results from reduced interactions with the mucus barrier due to two key features of LP-PEG: (i) the presence of a PEG corona, which provides steric hindrance and reduces adhesive interactions with mucins, and (ii) the negative surface charge imparted by DSPE-PEG, which contributes to electrostatic repulsion from the similarly negatively charged mucin network. This interpretation is supported by previous findings demonstrating that PEGylation of nanoparticles made of poly(lactic-*co*-glycolic acid) or lipids enhances mucus penetration and diffusion by minimizing adhesive and electrostatic interactions with mucosal components. [38,50,61] In contrast, unmodified LPs, which exhibit near-neutral zeta potential and lack PEGylation, are more likely to be trapped within the mucus mesh as has been previously demonstrated for DPPC coated NPs, [62] thereby limiting their diffusion and reducing their basolateral accumulation. The outermost hydrophilic and zwitterionic end of DPPC, the main lipid of LP, includes amino groups which can have attractive interactions with the electronegative mucins. [63]

Lung surfactant (LS) lines the alveoli and forms a pulmonary surfactant corona around NPs crossing the upper airway barrier. [19] This corona influences NP deposition, aggregation, drug release, and immune

Table 1
Top 10 proteins on the LS corona of LP and LP-PEG.

Top 10 LP coronal proteins			Top 10 LP-PEG coronal proteins	
Identified proteins	Accession	Relative proportion %	Identified proteins	Relative proportion %
Pulmonary surfactant protein A	F1SER3	14.5	*Pulmonary surfactant protein A*	13.2
Na(+)-dependent phosphate cotransporter 2B	F1S5A6	9.7	Na(+)-dependent phosphate cotransporter 2B	10.8
Actin gamma 1	A0A287A5G1	8.5	Actin gamma 1	8.6
Albumin	A0A286ZT13	5.9	Albumin	8.0
LanC like 1	A0A286ZXU8	5.7	LanC like 1	6.5
Pulmonary surfactant protein B	A0A287B0B8	3.7	*Pulmonary surfactant protein B*	3.3
Apolipoprotein A-I	K7GM40	3.5	GLOBIN domain	2.7
GLOBIN domain	F1RGX4	2.9	Apolipoprotein A	2.7
Pulmonary surfactant protein D	A0A5S6I5J5	2.9	Ig-like domain-containing protein	2.7
Ig-like domain-containing protein	F1RL06_PIG	2.5	*Pulmonary surfactant protein D*	2.5

response. [13,64] The corona's composition depends on NP surface chemistry and morphology, affecting the adsorption of surfactant proteins (SPs, such as SP-A, SP-B, SP-C, SP-D), known to orchestrate the fate of inhaled NPs and their immune responses. [18,20] Previously, our group used Magnetic Resonance Imaging (MRI) to show that NPs of similar size and charge, made from phosphatidylcholine (PC) or bovine serum albumin (BSA), had vastly different lung residence times, weeks for PC micelles and hours for BSA micelles. This difference was linked to SP-A interactions, which impact NP stability and opsonization. [22] Since LS corona effects are crucial for pulmonary drug delivery, studies integrating its complete analysis with NP lung biodistribution should be extended to predict the key features of inhalable nanomedicines.

We analyzed the protein composition of the LS corona by soft magnetic separation using the protocol of Raesch et al. [20] LPs were incubated with native porcine LS, one of the most complete surfactant preparations to predict nano-biointeractions with this lung fluid. [65] For this purpose, LPs were loaded with hydrophilic iron oxide NPs following the protocol of Fernández-Méndez et al. for magnetic separation, [66] maintaining similar d_H and zeta potential to PFD-loaded LPs (Fig. S2). Total protein quantification (Fig. 2D) confirmed that PEGylation reduced protein adsorption, which was consistent with the antifouling properties.

Proteomic analysis (Table 1) showed that both LS coronas shared similar major protein profiles, with SP-A, SP-B, and SP-D among the top ten most abundant proteins and no statistical difference in the abundance of SPs, as shown in Fig. S3A—C. SP-A was the most abundant protein in both LS coronas, unlike previously reported NPs, made of magnetite coated with PLGA, PEG, or lipids. [20] This likely results from SP-A's affinity for phospholipid membranes, [67] particularly if they are based on DPPC, [68] the main component of LP and LP-PEG.

SP-A plays a key role in opsonization, promoting phagocytosis and clearance of SP-A-bound particles, including microorganisms. [22] However, it is also involved in LS recycling and uptake by alveolar type II cells and alveolar macrophages (AM). [67] Nanoparticle coating with SP-A has been explored as a strategy to target these cell types following pulmonary administration, thereby enhancing drug retention. [22,69] SP-A has been shown to bind to PEGylated nanoparticles, [20] increasing the hydrodynamic diameter of the nanomaterials by less than 2 nm. [69] According to Palaniyar, [70] SP-A measures approximately 16–19 nm in length, suggesting that its interaction with PEGylated NPs is likely mediated *via* its collagen-like domain rather than the globular headgroup. Given that SP-A is an octadecamer with strong affinity for DPPC-containing membranes ($K_D = 4.3 \pm 0.2$ nM), [22] it is plausible that the collagenous domain facilitates simultaneous binding to both the PEG moiety and the sn-2-palmitate of DPPC. [71] These interactions likely contribute to the stable adsorption of SP-A irrespective of PEGylation, which may explain its similar presence on both lung surfactant coronas.

SP-B, a hydrophobic, positively charged surfactant protein of the saposin-like family, promotes membrane aggregation primarily acting at the surface of membranes. [72] Its presence in both LS coronas suggests it may facilitate phospholipid membrane reorganization, as previously observed for lipid NPs in cryo-TEM studies by Foged et al. [73]

Finally, SP-D, with high affinity to hydrophilic surfaces, was also highly abundant in both the LS coronas of LP and LP-PEG. This protein like SP-A is highly involved in defining the fate of NPs in the lungs, since it is involved in the defense mechanisms and clearance of external bodies from the lungs but also in the surfactant homeostasis and recycling. [67]

Coating of NP surfaces with SPs, such as SP-A or SP-D, has often been associated with enhanced lung clearance by immune cells. [74,75] However, the formation of the LS corona or LS surface coating has also been proposed as a "camouflage" that may evade the pulmonary immune system and increase NP retention time in the lung. [76,77] To gain insight into the potential camouflaging effect, the similarity of the LS coronas formed in LP and LP-PEG to the native LS was investigated. First, the SPs were analyzed. Fig. 2E shows that both PEGylated and non-PEGylated LPs had similar relative proportions of SPs that closely matched those of native LS, except for SP-C, which was significantly lower in both cases (Fig. S3F). SP-C is a highly hydrophobic protein that acts in cooperation with SP-B in promoting the surface tension reduction capabilities of LS, but with a greater contribution to transmembrane interactions. Its low presence in the LS corona of both LPs suggests that SP-C may have a low effect on the permeability and packing of the phospholipid bilayers of LPs as it normally does in LS membranes. [78] Overall, our data suggest that the DPPC-based composition of liposomes plays a dominant role in shaping the surfactant corona by supporting native lipid–protein interactions. This property can be harnessed in drug delivery strategies to enhance pulmonary targeting and retention, as shown in previous studies, although surfactant corona formation was not explicitly examined in those cases. [79,80]

To further assess the impact of PEGylation on other functional proteins comprising the LS coronas, 1973 proteins were detected and categorized into functional groups based on gene names and descriptions (functional groups are described in the SI). The mean fold changes were calculated for each protein category, and proteins with significant differences were identified. Differential expression analysis based on $\log_2$ fold changes, defined significant changes as $|\log_2 FC| > 0.5$. Fig. 2F shows that PEGylation had a negligible impact on the adsorption of antifouling, immunological, metabolic, signaling, structural, transport, and surfactant proteins. However, inflammatory and cell adhesion proteins were modestly reduced in LP-PEG compared to those in the LP corona. PEGylation is commonly used to minimize the levels of inflammatory proteins in intravenously administered NPs. This effect appears to extend, albeit modestly, to the LS corona. A lower abundance of cell adhesion proteins generally reduces nanoparticle-cell interactions and uptake.

To correlate the proteomic results with their impact on cellular uptake in the presence and absence of native LS, we performed flow cytometry using fluorescently labeled LP or LP-PEG on alveolar epithelial cells (A549), profibrotic macrophages (THP1), and human primary lung fibroblasts (HLF) activated with different growth factors to

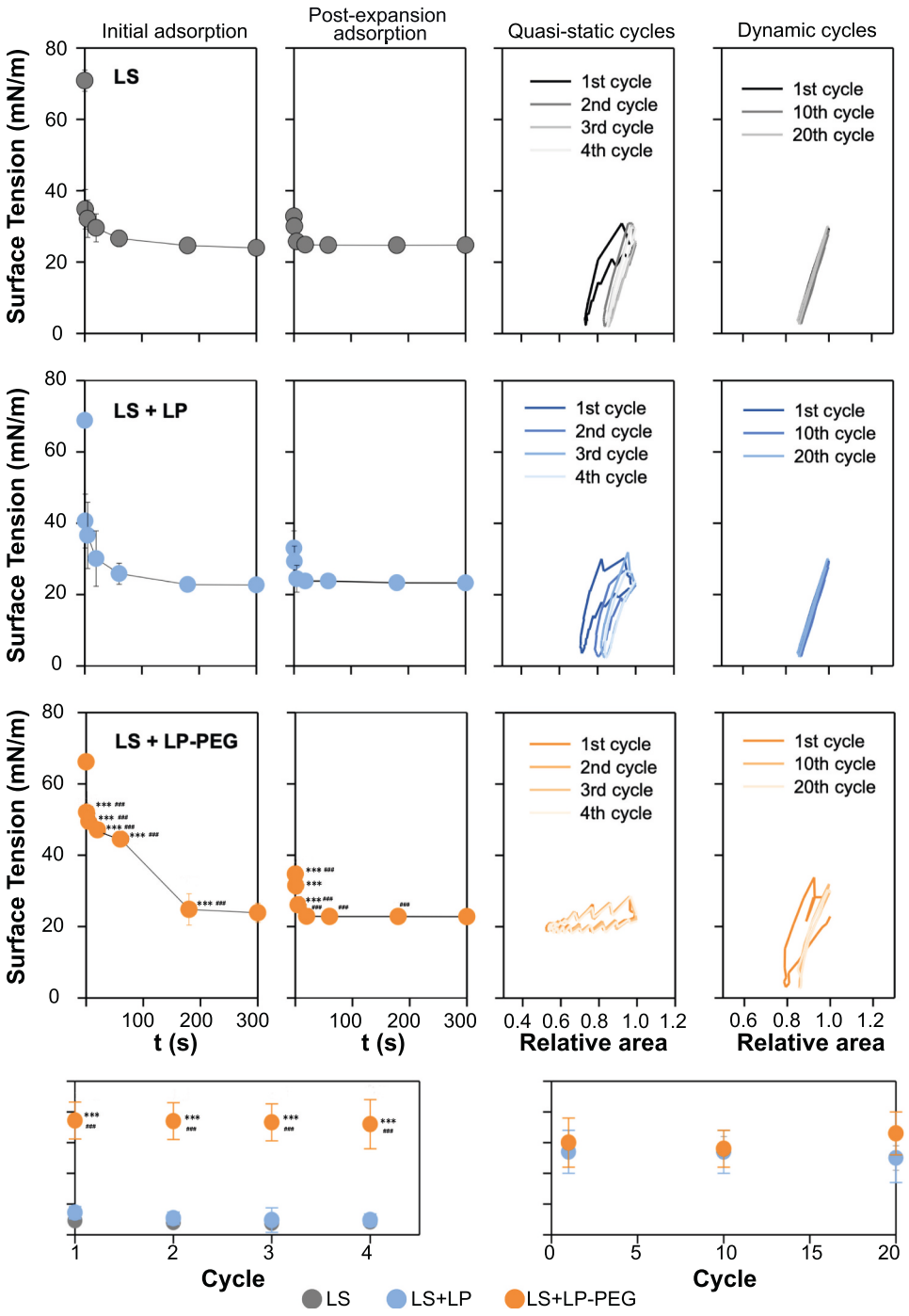

Fig. 3. Effect of PEGylation on the functional properties of native LS. (A) Initial adsorption (left), post-expansion adsorption (center left), and quasi-static (center right) and dynamic (right) compression-expansion cycles of LS alone (upper row) and in the presence of 10 % (*w*/w) LP (central row) or LP-PEG (lower row) measured using a captive bubble surfactometer. (B) Minimum surface tensions attained upon quasi-static cycling as a function of the cycle number. (C) Dependence of the minimum surface tensions attained during dynamic cycling on the cycle number. ($n = 5$). Differences in means between groups were evaluated by one-way ANOVA followed by the Holm-Sidak multiple-comparison test using Sigma-Plot. A *p*-value <0.001 was obtained for LP-PEG when compared with LP (***) and LS ($^{\#\#\#}$).

resemble fibrotic tissue. PEGylation reduced LP mean fluorescence intensity (MFI) within cells in the absence of LS after 4 and 24 h (Fig. 2G and S4A) in A549, THP1, and HLF cells. This finding aligns with the steric hindrance and hydrophilicity of PEG, which hampers interactions with cell surface receptors and proteins. [81] However, the impact of the LS corona on cellular uptake varied across different cell types. Macrophages showed no significant change in either MFI (Fig. 2G) or the percentage of positive cells in the presence of LS (Fig. S4B). In contrast, in A549 and HLF cells, the LS corona reduced the uptake of non-PEGylated LPs, whereas PEGylated LPs exhibited similar MFI in the three cell types regardless of the presence of LS. In the three cell lines studied, PEGylation hampered the influence of LS on cellular uptake. Interestingly, when comparing the percentage of positive cells (Fig. S4B), we observed that HLF exhibited a higher percentage of LP-PEG-positive cells decorated with the LS corona than those incubated with bare LP-PEG.

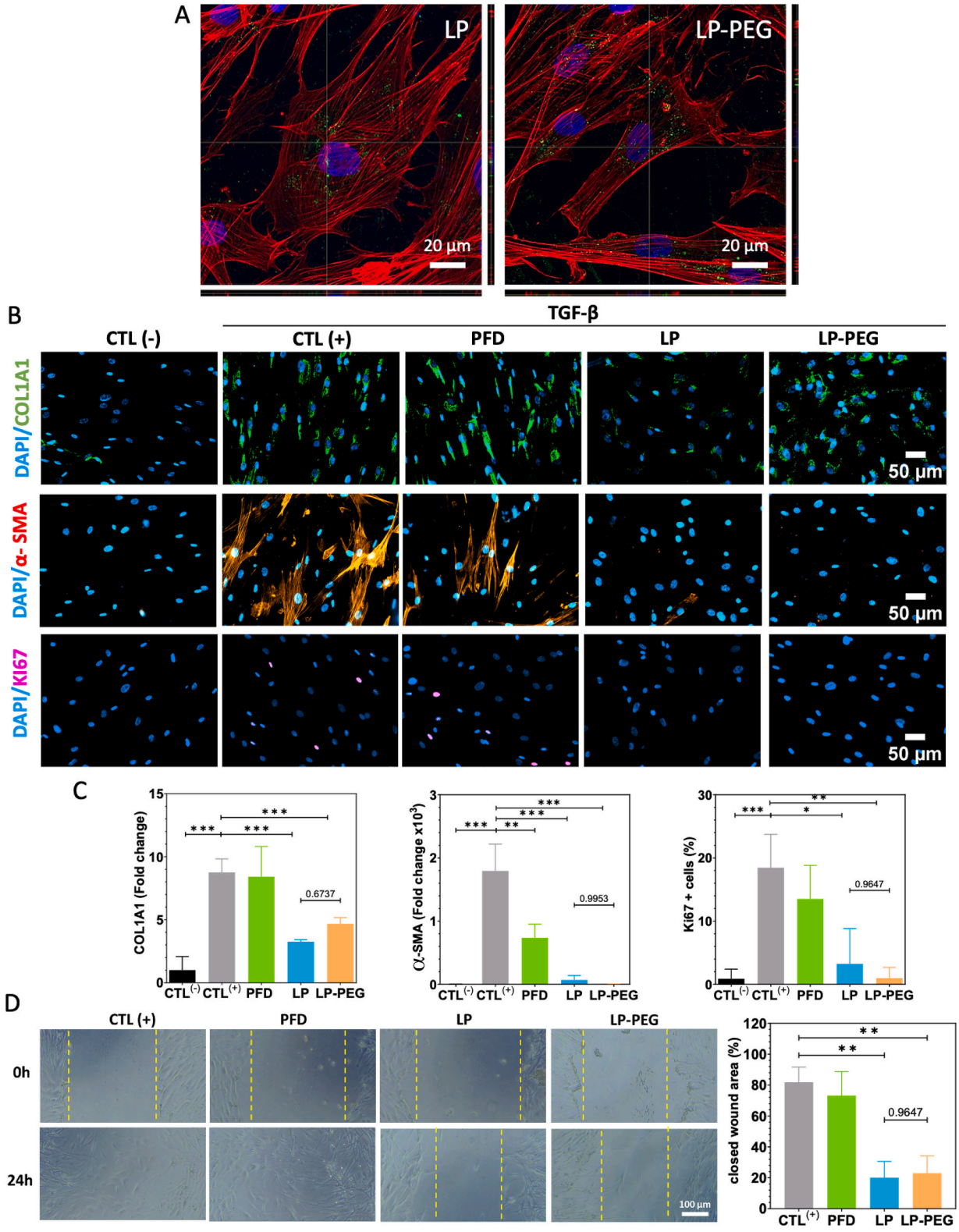

Fig. 4. *In vitro* evaluation of the therapeutic effect of PFD encapsulated in LP and LP-PEG. (A) Confocal images of TGF-β1 activated HLFs after incubation with $DiOC_{18}$ (484/521 nm) labeled LP and LP-PEG. The cell nucleus is shown in blue, the acting cytoskeleton is shown in red, and LP and LP-PEG are shown in green. (B) Representative immunofluorescence images of COL1A1 (green), α-SMA (red), and Ki-67 (pink) staining (co-stained with DAPI, blue) of HLFs activated with TGF-β1 (CTL $^{(+)}$) and treated with free PFD, PFD-LP, and PFD-LP-PEG compared with non-activated HFLs (CTL$^{(-)}$). (C) Quantitative analysis of COL1A1, α-SMA, and Ki67 immunostaining images shown in (B). (D) Representative optical images from the cell migration assay of TGF-β1-activated HLFs without treatment (CTL $^{(+)}$) and treated with free PFD, LP, or LP-PEG, along with quantification of the closed scratched area after 24 h. $n = 3$; data represent mean ± SD. Statistical analysis was performed using one-way ANOVA with Tukey's multiple comparison test (*$p < 0.05$, **$p < 0.01$,***$p < 0.001$). The experimental details are provided in the Supporting Information (SI). (For interpretation of the references to colour in this figure legend, the reader is referred to the web version of this article.)

These findings suggest that PEGylation primarily acts by hindering LP internalization but also attenuates the influence of the LS corona on cell uptake. The observed reduction in NP uptake due to LS corona formation is consistent with previous studies. [77,82,83] Although counterintuitive for LP and LP-PEG given the presence of SP-A, SP-B, and SP-D in the LS corona (reported to enhance cell internalization), [13] Bai et al. have recently suggested a slowing down of the endocytosis process due to the high lipid density of the LS corona of lipid NPs. [84] The presence of PEG on the surface of the LPs may prevent the densification of their LS corona, thus avoiding this effect. To the best of our knowledge, few studies have comprehensively correlated the full protein composition of the LS corona, with cellular uptake in alveolar cells. However, these studies are essential to determine whether nano-biointeractions can be reliably predicted using proteomic analyses.

In drug delivery with inhalable nanocarriers, such as PFD-loaded LP and LP-PEG, the formation of the LS corona may also influence the release and diffusion of the encapsulated drug. To assess how PEGylation affects this release, we analyzed the temporal delivery of PFD during the dialysis of LP and LP-PEG in the presence and absence of native LS. The results of this analysis showed that LP-PEG exhibited a slightly faster (but not significantly different) release profile than LP both in the presence and absence of native LS (Fig. 2H, Fig. S5) resulting in a similar retention of the encapsulated PFD. These findings suggest that LS corona formation has a negligible effect on the drug stability of both PEGylated and non-PEGylated LPs for sustained drug delivery.

In addition to evaluating the effects of the LS corona on cellular uptake and drug delivery, it is crucial to assess the potential impact of LPs on native LS performance, as interactions between NPs and LS can

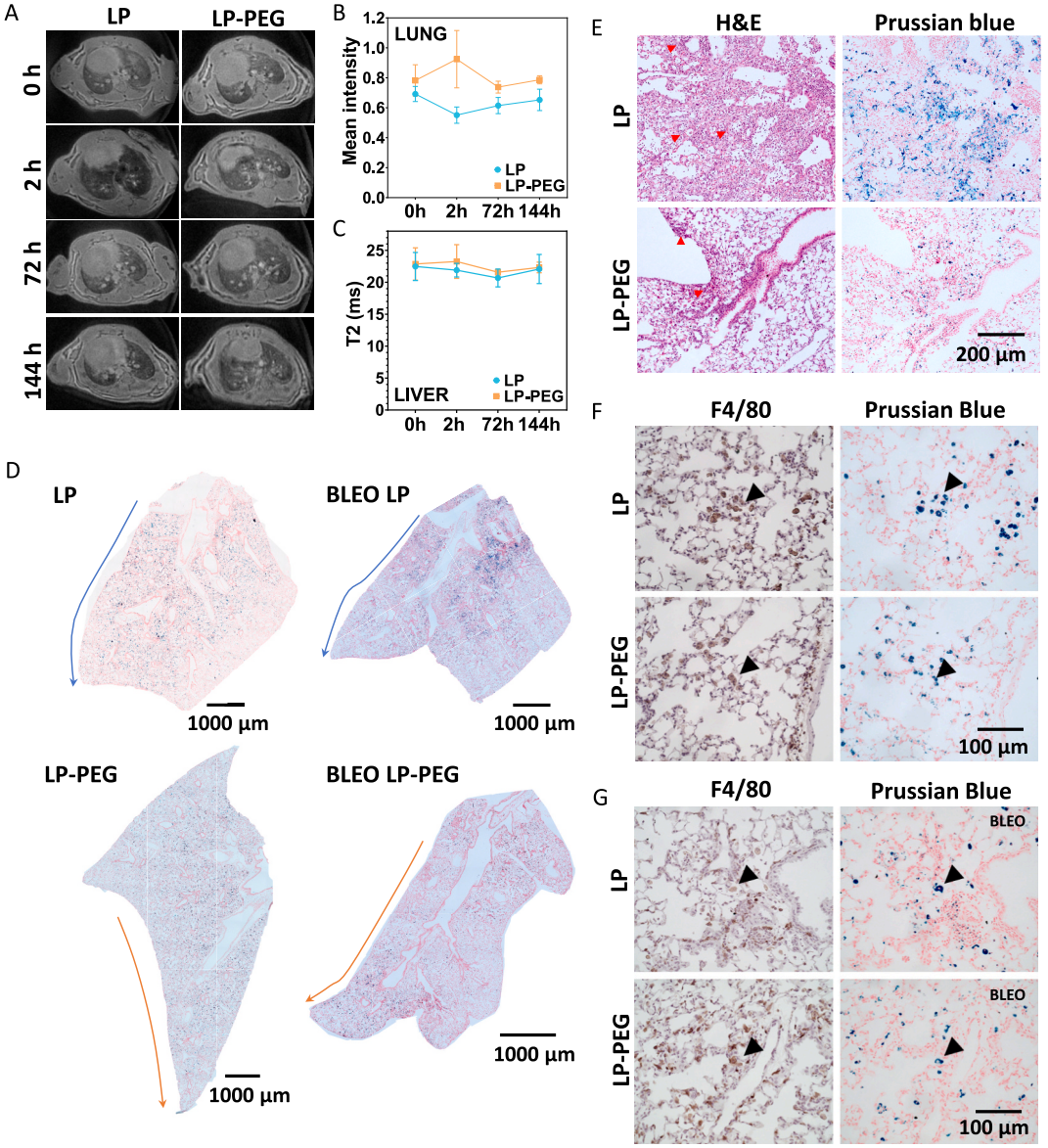

Fig. 5. *In vivo* biodistribution and lung retention study of LP and LP-PEG. (A) Coronal UTE3D MRI of the lungs taken before IT administration of LP and LP-PEG (loaded with IONP) and at 2-, 72-, and 144-h post-administration. (B) Mean MRI intensity in lung tissue. (C) Quantification of MRI T_2 (ms) values in the liver. (D) PB staining of the lung lobes of healthy mice and BLEO mice after IT administration of LP and LP-PEG. Arrows indicate the penetration of LPs into the lung lobe (healthy lungs in blue and fibrotic lungs in orange). (E) PB and H&E staining of lung areas with high cellular infiltration in BLEO mice showing the presence of both LPs in the fibrotic regions. F4/80 immunohistochemistry and PB staining of the lungs after LP and LP-PEG administration in healthy mice (F, 6-days post IT administration) and BLEO mice (G, 24-h post IT admin.). Black triangles indicate matched cells in both types of stains. Red arrows indicate eosinophilic structures marked in red such as collagen fibers in the extracellular matrix. (For interpretation of the references to colour in this figure legend, the reader is referred to the web version of this article.)

lead to surfactant depletion and lung toxicity, [72] a phenomenon observed with certain NPs, such as those made of hydroxyapatite. [85,86] Given that inhaled materials may interfere with the endogenous surfactant system and inhibit its biophysical function, we investigated the interactions between LP and LP-PEG with native LS using a captive bubble surfactometer which allows us to determine the potential disruption of LS surfactant function. [43,44] Fig. 3 indicates that LP-PEG, unlike LP, impaired the initial adsorption of LS, thereby increasing the time required to reach equilibrium surface tension (23.5 ± 0.7 mN/m) without significantly affecting post-expansion adsorption (Fig. 3A). Additionally, as shown in Fig. 3A, the interaction between LS and PEGylated liposomes prevented the surfactant from reducing the surface tension to near-zero values during quasi-static compression. The persistence of this inhibitory effect upon cycling (Fig. 3B) suggests that the LP-PEG liposomes remained associated with the surfactant film and were not excluded during slow compression/expansion cycles. When cycled at physiological rates, LS reduced the surface tension to very low values in the presence of both types of particles (Fig. 3C). However, for the LS/LP-PEG mixture, an increase in hysteresis during the first cycle was observed, along with a gentler slope in the surface tension-relative area plot at higher cycle numbers (Fig. 3A), indicating the LP-PEG-induced fluidization of the LS film. This fluidization can have significant physiological consequences, including increased surface tension, reduced lung compliance, and potential respiratory distress, which may impair gas exchange or contribute to inflammation and lung injury. [87] The impact of NP PEGylation on LS interactions is often overlooked but warrants in-depth investigation, as its long-term effects may have important health implications. [72].

3.3. Role of PEGylation in the in vitro therapeutic effects of PFD-loaded LPs

Profibrotic alveolar fibroblasts play a central role in PF by overproducing extracellular matrix (ECM) components and inducing tissue remodeling. These fibroblasts undergo abnormal differentiation into myofibroblasts, which are apoptosis-resistant, more invasive than non-activated fibroblasts, and overproduce type I, III, and IV collagen, among other ECM components. [88] To assess whether PEGylation influences the therapeutic efficacy of PFD-loaded liposomes, we utilized transforming growth factor beta 1 (TGF-β1)-activated HLFs. TGF-β1, a key profibrotic cytokine, promotes collagen synthesis, myofibroblast differentiation, cell proliferation, and migration. [8] We then compared the antifibrotic effects of PFD-loaded LP and LP-PEG.

We first confirmed the low cytotoxicity of LPs in alveolar cells (Fig. S6A) and the internalization of LP and LP-PEG labeled with $DiOC_{18}$ in TGF-β1-activated HLFs, A549 and THP-1 observing their perinuclear localization, which is characteristic of endocytosed nanoparticles (Fig. 4A, Fig. S6B,C). [89] Flow cytometry analysis after 4 h of LP incubation revealed a similar percentage of positive cells but significantly lower MFI of LP-PEG compared with LP suggesting their lower internalization, as observed in confocal images for the three cell types, HFL, A549 and THP-1 (Fig. S4, Fig. S6D).

Next, quantitative immunofluorescence analysis (Fig. 4B, C) was performed to assess key profibrotic markers in TGF-β1-activated HLFs, including collagen type I (COL1A1), α-smooth muscle actin (α-SMA), and Ki-67, a nuclear protein associated with cellular proliferation. After incubation with PFD-LP and PFD-LP-PEG, no significant difference was observed in the reduction of fibrotic markers between PEGylated and non-PEGylated LPs, despite lower cell internalization (Fig. 2G, Fig. S4). However, both LP formulations exhibited significantly higher efficacy than free PFD. The lack of a therapeutic effect of empty LPs has been demonstrated and is shown in Fig. S7.

A similar trend was observed in the cell migration assay (Fig. 4D). Time-lapse imaging of wound closure in TGF-β1-differentiated HLF monolayers showed that encapsulated PFD, whether in LP or LP-PEG, outperformed free drug in suppressing fibroblast migration. No significant difference in efficacy was observed between LP and LP-PEG formulations after 4 h of treatment. These findings suggest that once a certain intracellular threshold concentration of PFD is reached, additional uptake does not proportionally enhance the therapeutic effect. This supports the notion of a nonlinear relationship between intracellular PFD concentration and therapeutic effect, characterized by a saturation plateau beyond which higher intracellular levels yield diminishing returns. This phenomenon aligns with clinical data showing that PFD efficacy in PF patients does not increase linearly with dose. [90] For instance, both lower (<1200 mg/day) and higher doses have demonstrated comparable clinical benefits, particularly in slowing lung function decline. These findings highlight the importance of maintaining PFD levels within a therapeutic window, where further increases in drug concentration offer limited incremental benefit. In our *in vitro* model, as in clinical practice, therapeutic optimization may depend more on achieving and maintaining effective intracellular concentrations than on maximizing uptake *per se*.

3.4. Role of PEGylation in lung retention time and biodistribution of LPs

Lung clearance of NPs is a significant challenge for pulmonary drug delivery, often resulting in rapid clearance or failure to reach deep regions of the lung. [91] Recent research suggests that fibrosis originates in the distal regions of the lung, where scar tissue tends to accumulate. Therefore, the design of drug nanocarriers capable of reaching these distal areas is crucial. [9]

To investigate the distribution and retention of LP and LP-PEG in the lung after pulmonary administration, we combined molecular imaging analysis using MRI with histological analysis of lung tissue in both healthy and fibrotic mouse models. In this study, IONP-loaded LP and LP-PEG were used, and their relaxivity properties are listed in Table S1. First, LP-IONP or LP-PEG-IONP were administered intratracheally (IT) to healthy mice, and MRI scans were performed before administration and at 2-, 72-, and 144-h post-administration (Fig. 5A). IT in mice is a widely used technique for administering substances directly into the lung and studying local effects, including the evaluation of nanomedicines intended for pulmonary administration. This route allows for precise distribution of the compound in deep lung tissue, facilitating the evaluation of the efficacy and toxicity of the administered nanoparticles or drugs. [92–94]

LP distribution in the lungs was assessed using ultra-short echo time MRI. To minimize motion artifacts associated with inhalation and exhalation, data acquisition was performed using respiratory gating, as previously reported, and the mean lung intensity was quantified. In these images, the mean lung intensity decreased with the accumulation of LPs (which exhibited T_2 MRI contrast) and increased with the accumulation of LP-PEG (which exhibited T_1 MRI contrast), confirming a high accumulation of both LPs in the lung tissue (Fig. 5B). At 72 and 144 h, the mean MRI intensity returned to baseline, indicating either massive aggregation of LPs or their clearance from the lungs. T_1 and T_2 parametric maps of the liver (Fig. 5C, Fig. S8A,B) and kidneys (data not shown) confirmed that IONPs were not systemically distributed in the blood, either within the LPs or as free NPs. These results were further validated through Prussian blue staining, which revealed a high accumulation of IONPs in the lungs but no detectable presence in other organs (Fig. S8C). In addition, PEG-free LPs exhibited a distribution pattern similar to that of LP-PEG, effectively reaching the distal lung regions as we observed in different lung lobes (Fig. 5D). This similar LP and LP-PEG biodistribution pattern was also observed in mice with bleomycin (BLEO)-induced pulmonary fibrosis suggesting a negligible influence of PEG on the retention time and distribution of LPs both in healthy and diseased lungs (Fig. 5D). In the fibrotic lungs, the IONP loaded in either LP or LP-PEG reached areas with high cellular infiltration characteristic of PF (Fig. 5E and Fig. S9), [95] and in both healthy and diseased lung tissue we observed the colocalization of delivered IONP with alveolar macrophages stained with the antibody F4/80

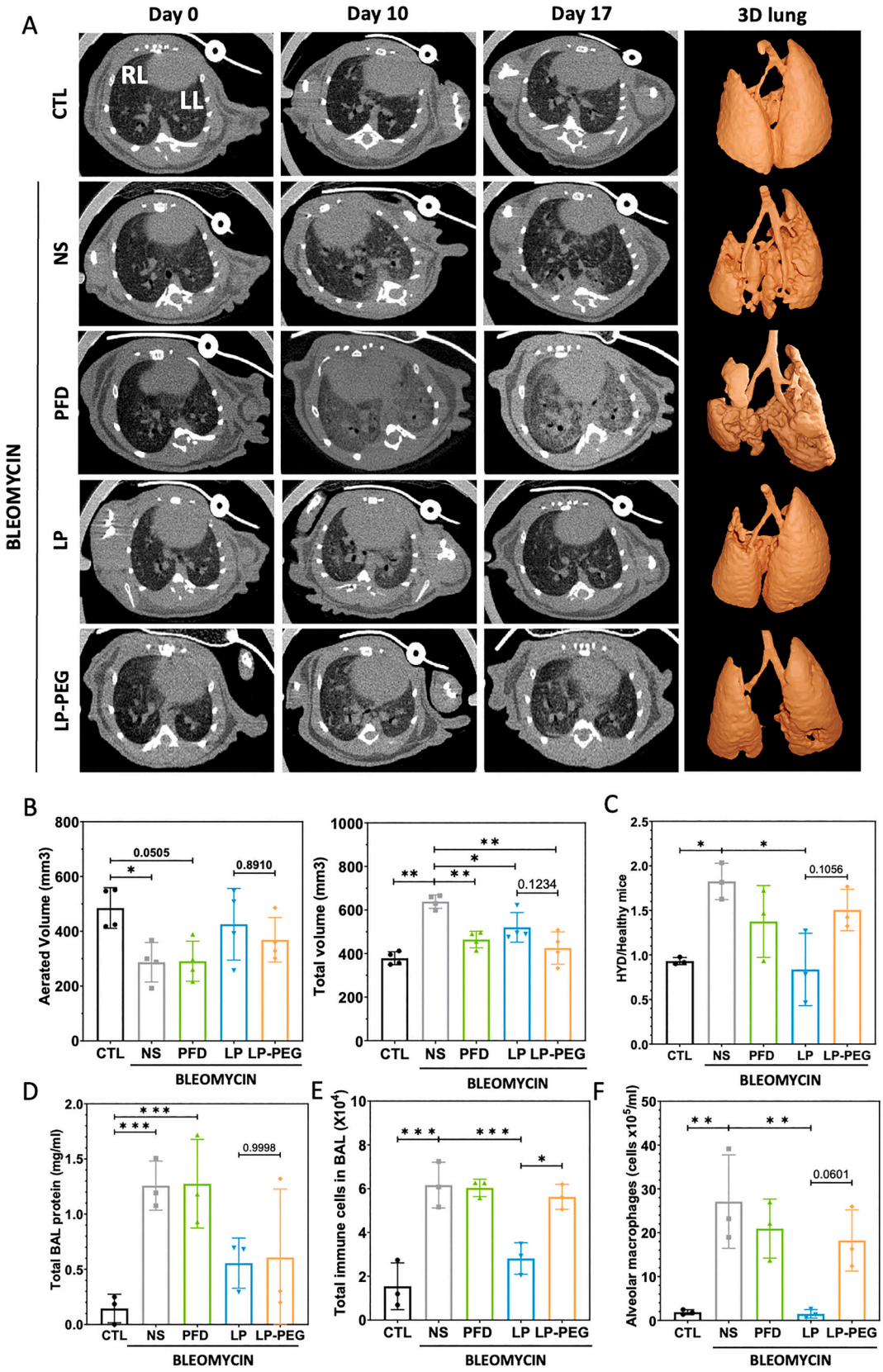

Fig. 6. *In vivo* study of the therapeutic effect of PFD encapsulated in LP and LP-PEG in the BLEO mouse model of PF. (A) Lung respiratory-gated CT of PF progression in mice at days 0, 10 and 17 following BLEO IT administration, along with 3D reconstructions of CT images at day 17 (right side). Mice were treated on days 10, 14 and 17 *via* IT administration of normal saline (NS), PFD, LP-PFD and LP-PEG-PFD. Untreated mice (CTL) were used as controls. (B) Quantification of aerated lung volume and total lung volume based on CT image analysis on day 17. (C) Quantification of hydroxyproline in *ex vivo* lung tissues. (D) Total protein quantification in BAL fluid. (E) Quantification of total immune cells in BAL on day 21 by flow cytometry. (F) Alveolar macrophage quantification in BAL on day 21 by flow cytometry.

Data are presented as mean ± SD; statistical analysis was performed using one-way ANOVA with Tukey's multiple comparison test (*$p < 0.05$, **$p < 0.01$,***$p < 0.001$).

(Fig. 5F,G and Fig. S9). These findings indicate that neither LP nor LP-PEG translocated into the bloodstream and remained in the lungs for extended periods. PEGylation of liposomes did not enhance their biodistribution within the lung or facilitate deeper penetration into the distal airways and fibrotic regions. Furthermore, PEGylation did not prevent the internalization of liposomes by alveolar macrophages, although it is possible that uptake occurred at reduced levels or with slower kinetics, as previously reported in other cell types.

Studies using fluorescent liposomes suggest that PEGylation improves NP penetration by increasing mucus diffusion and reducing alveolar cell uptake. [7,96] However, PEG-free phospholipid-coated NPs have also shown long-term retention in distal lung regions. [22,62] Recent DPPC-based lipid NP studies indicate that PEG-free formulations stable in inhalation devices may achieve comparable lung distribution and drug delivery efficiency. [97] This raises the question of whether PEG is essential for inhaled nanomedicines.

PEGylation stabilizes formulations for dry powder or nebulized delivery, but aerodynamic properties and stability depend on the inhalation device between other factors such as viscosity. [98] Most current devices cause lipid NP aggregation or degradation. However, emerging strategies, such as charge-assisted stabilization, are improving nebulized lipid NP stability beyond PEGylation and could be used in future PEG-free inhalable formulations. [99,100]

3.5. Role of PEGylation in the therapeutic effect of PFD-loaded LPs in vivo

To assess the impact of PEGylation on PFD-loaded DPPC-based LPs, a BLEO mouse model was used. Ten days post-BLEO, fibrosis was confirmed by histology and increased lung SUV of [^{68}Ga]-FAPI-46 on PET/CT (Fig. S10). This biomarker enables non-invasive fibrosis monitoring, even in early stages. [101] CT scans also showed higher mean Hounsfield unit (HU) density (Fig. S11A), reduced aerated lung volume (from −900 to 300 HU), and increased total lung volume, consistent with fibrosis. [102]

With fibrosis established, treatments began on day 10 post-BLEO, consisting of three IT administrations (days 10, 14, and 17) of 4.2 mg/kg PFD, either free or encapsulated in LP or LP-PEG. Therapeutic effects were monitored using CT imaging until day 21. CT 3D reconstructions (Fig. 6A) and analysis (Fig. 6B) confirmed significant reductions in aerated lung volume and increased total lung volume in BLEO-treated mice compared to controls (CTL). Treatment improved aerated lung volume, with LP-PFD showing the greatest effect, followed by LP-PEG-PFD and free PFD. However, the total lung volume decreased similarly across all treatments. MRI analysis further indicated no additional antifibrotic benefits of PEGylation (Fig. S12).

Ex vivo analyses were performed to validate CT imaging results. Hydroxyproline quantification (Fig. 6C) confirmed that LP-PFD was the most effective treatment for reducing collagen content, outperforming free PFD and LP-PEG-PFD. To assess the impact of PEGylation on the antifibrotic effect of encapsulated PFD, bronchoalveolar lavage (BAL) was conducted at the study endpoint. Total BAL protein, which is typically elevated in PF, [7,8] was similarly reduced by PFD-loaded liposomes (LP and LP-PEG) but not by free PFD (Fig. 6D). Flow cytometry revealed a reduction in infiltrated immune cells, with LP-PFD being the most effective treatment (Fig. 6E). Among these immune cells, alveolar macrophages (Fig. 6F) and alveolar lymphocytes (Fig. S11B) were significantly reduced in mice treated with LP-PFD, whereas this decrease was much less pronounced with LP-PEG-PFD. Overall, PEGylation did not enhance the antifibrotic effects of PFD-loaded liposomes and, in fact, diminished their anti-inflammatory efficacy. This reduced efficacy in the LP-PEG group may be attributed to impaired interactions between the PEGylated liposomes and alveolar cells, leading to limited uptake by key immune and epithelial cells. Consequently, local drug concentrations at sites of inflammation and fibrosis may fall below the therapeutic threshold.

In contrast, non-PEGylated LPs are more efficiently internalized by alveolar macrophages and epithelial cells, resulting in higher local accumulation of PFD and a more sustained therapeutic effect. These properties likely account for the more pronounced reductions in immune cell infiltration, protein leakage, and collagen deposition, evidenced by lower hydroxyproline levels, observed in the LP group.

These findings align with previous studies demonstrating that the therapeutic efficacy of PFD is enhanced when delivered *via* non-PEGylated nanoparticles, due to improved cellular uptake and retention within lung tissue. [103] Overall, the discrepancy between LP and LP-PEG groups highlights the critical role of nanoparticle surface characteristics in determining the therapeutic performance of inhaled PFD formulations.

To confirm the findings from molecular imaging, hydroxyproline levels, and BAL analysis, we performed histology and immunofluorescence on lung tissue to assess fibrotic markers. H&E, Masson's trichrome (TM), and Picrosirius red (PR) staining (Fig. 7A) showed that PFD-loaded LP and LP-PEG significantly reduced BLEO-induced PF severity compared to free PFD. Quantification of the collagen area by PR staining, as well as COL1A1 and α-SMA immunofluorescence (Fig. 7B-E), further confirmed that both LP treatments decreased these fibrotic markers more than free PFD. However, histological and immunofluorescence results indicated negligible differences between the PEGylated and PEG-free LPs, similar to the CT results.

In addition, we confirmed that no antifibrotic effects were observed in the empty LP or LP-PEG controls (Fig. S11C). To evaluate the potential adverse effects of the LP and LP-PEG formulations, we monitored the animal weight every three days. Both LP and LP-PEG-treated animals showed weight increases similar to those of healthy controls (Fig. S11D), unlike the significant weight loss observed in saline-treated controls.

4. Conclusions

In this study, we explored the role of PEGylation in enhancing liposome performance for pulmonary delivery in pulmonary fibrosis. This study was conducted on multiple scales, aiming to connect and correlate results ranging from nano-biointeraction studies with lung fluid surrogates and proteomic analysis of the pulmonary surfactant corona to biodistribution studies in healthy and fibrotic lungs and therapeutic effects *in vitro* and *in vivo*. Although these studies should be extended to different PEG percentages, molecular weights, and types of nanoparticles, our findings provide valuable insights into the nuanced effects of PEGylation on the behavior of liposomal formulations and their interactions with the unique microenvironment of the lungs.

We confirmed that PEGylated liposomes, likely holding a brush like configuration, facilitated mucus diffusion, a crucial step for effective pulmonary delivery in pulmonary fibrosis and modestly reduced the presence of inflammatory proteins in the corresponding lung surfactant corona. This suggests the potential benefits of mitigating inflammatory responses. Additionally, PEGylation led to a reduction in cell adhesion proteins within the lung surfactant corona, which may have decreased cellular uptake. These results were further evaluated *in vitro* using different alveolar cell types, confirming the lower uptake of PEGylated liposomes by alveolar macrophages, epithelial cells, and fibroblasts following lung surfactant corona formation.

Despite the differences in cell adhesion and inflammatory proteins between the lung surfactant corona of PEG-free and PEGylated liposomes, most functional proteins, including lung surfactant proteins

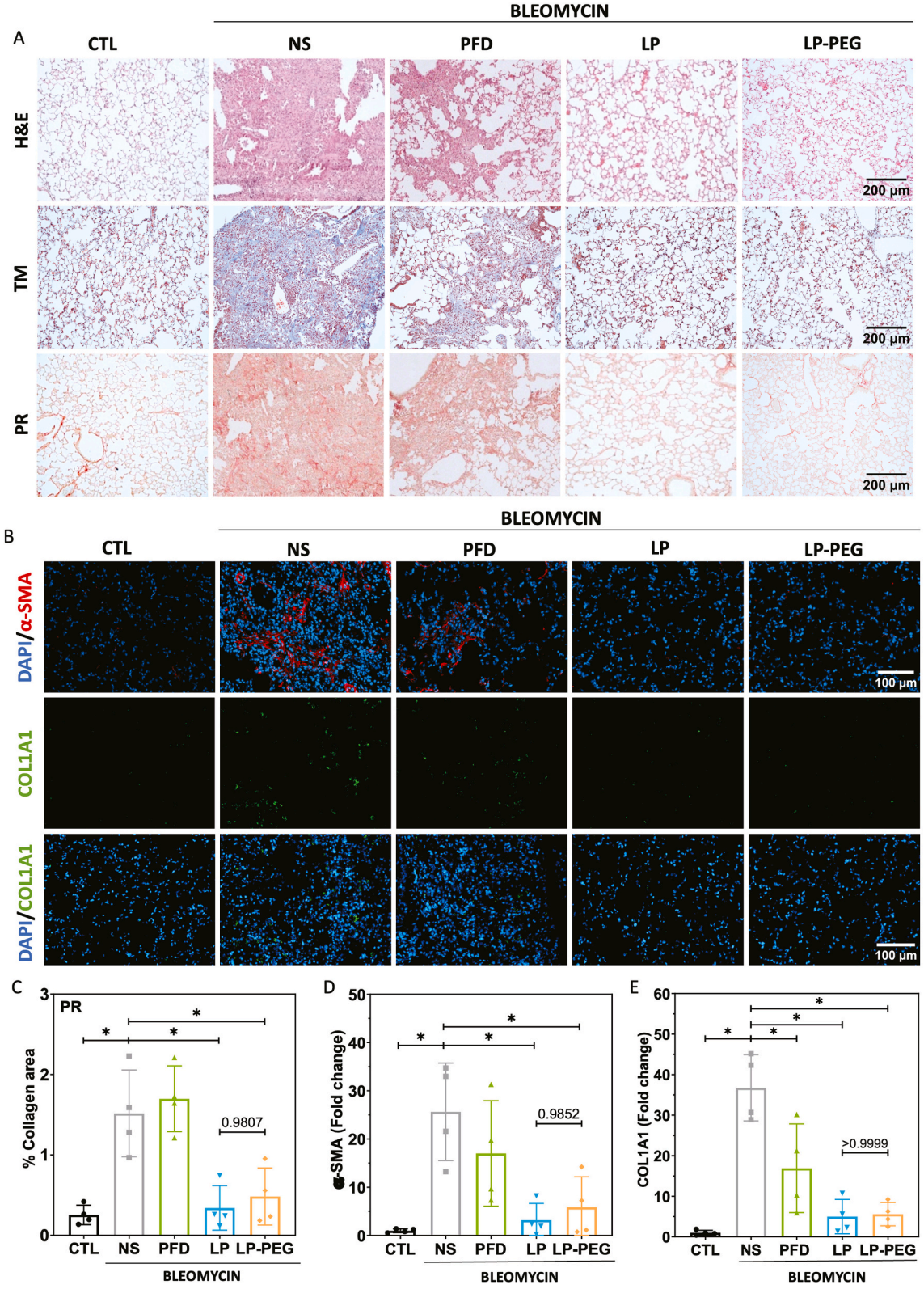

Fig. 7. Histological analysis of lung tissue in the BLEO mouse model of PF. (A) Representative images of H&E, Masson's trichrome (TM), and Picrosirius Red (PR) staining of lung sections following three IT administrations of normal saline (NS), PFD, LP-PFD, and LP-PEG-PFD. Mice without BLEO administration served as control (CTL). (B) Representative immunofluorescence images of α-SMA and COL1A1 co-stained with DAPI. (C) Quantitative analysis of the collagen area in PR-stained lung sections. (D, E) Quantitative analysis of COL1A1 and α-SMA immunofluorescence staining. Data are presented as mean ± SD; statistical analysis was performed using one-way ANOVA with Tukey's multiple comparison test (*$p < 0.05$). (For interpretation of the references to colour in this figure legend, the reader is referred to the web version of this article.)

known to orchestrate particle fate in the lungs, were similarly abundant. This could explain the comparable biodistribution and lung retention times observed for both liposomes in MRI and histological analyses of healthy and fibrotic lungs. Future research should investigate the underlying reasons for these similarities in the lung surfactant corona and whether they are attributable to the high DPPC content or the type of PEGylation used. Moreover, additional studies combining lung surfactant corona analysis with nanoparticle biodistribution assessments after pulmonary administration are needed to determine to what extent biodistribution and retention time in the lung can be predicted from proteomic data.

Beyond studying the impact of the lung surfactant corona on antifibrotic liposomes, we also evaluated the effect of these liposomes on the biophysical properties of this fluid, which is essential for lung function. Surprisingly, PEGylated liposomes temporarily increased lung surfactant fluidity, potentially leading to detrimental effects. Further research should comprehensively evaluate the influence of PEG density, along with other parameters such as molecular weight, on the biophysical properties of lung surfactant. It is essential to determine whether these effects are reversible or persistent in order to properly assess the risk associated with this previously overlooked phenomenon.

Despite improvements such as enhanced mucus penetration, PEGylation did not significantly increase the lung retention time or biodistribution of liposomes in fibrotic lungs, which are key factors for sustained drug delivery. Consequently, when assessing the antifibrotic effects of PEG-free and PEGylated pirfenidone-loaded liposomes *in vivo*, PEGylation did not enhance therapeutic efficacy. Instead, it attenuated the effect of the drug in reducing immune cell infiltration in the lungs and protein content in the bronchoalveolar lavage fluid.

In conclusion, for the DPPC-based liposomes studied, by performing a multiscale analysis we determined that the overall benefit of PEGylation in enhancing nano-biointeractions appeared limited, as demonstrated by our assays involving lung surfactant, alveolar cells and lung tissue. Future studies should thoroughly explore the interplay between different types of PEGylation and liposomes, surfactant interactions, immune responses, de-PEGylation in the lung environment, and drug efficacy to fully evaluate the advantages and limitations of PEGylation for pulmonary administration.

CRediT authorship contribution statement

Marina Piñol-Cancer: Writing – original draft, Methodology, Investigation, Formal analysis, Data curation, Conceptualization. **Laura Fernández-Méndez:** Methodology, Formal analysis, Data curation. **Juliana Carrillo-Romero:** Investigation, Formal analysis, Data curation. **Ainhize Urkola-Arsuaga:** Investigation, Data curation. **Mikel Azkargorta:** Investigation, Formal analysis, Data curation. **Félix Elortza:** Supervision, Methodology, Formal analysis. **Felipe Goñi-de-Cerio:** Supervision, Methodology, Formal analysis. **Cristina García-Mouton:** Methodology, Investigation. **Claudia Miranda-Pérez de Alejo:** Validation, Software, Methodology, Investigation. **Ermal Ismalaj:** Methodology, Investigation. **Olga Cañadas:** Writing – original draft, Supervision, Investigation, Formal analysis. **Jesús Pérez-Gil:** Visualization, Validation, Supervision, Resources, Methodology, Conceptualization. **Susana Carregal-Romero:** Writing – review & editing, Writing – original draft, Visualization, Supervision, Resources, Project administration, Funding acquisition.

Declaration of competing interest

The authors declare no conflict of interest.

Acknowledgements

SCR acknowledges the MCIN/AEI 10.13039/501100011033 projects (PID2019-106139RA-100, CNS2023-143944, RYC2020-030241-I, PID2022-142842OB-I00), and the Ramón Areces Foundation (CIVP21S13151). JRC is funded by MCIN/AEI/10.13039/501100011033 (PID2021-123238OB-I00), the Basque Government under the Elkartek 2024 Program (bmG24), and R&D projects in Health (Grant number 2022333041). SCR and JRC thank IKERBASQUE for sponsoring them. We also acknowledge the "Fundación contra la hipertensión pulmonar" for funding (Empathy). JPG acknowledges the Spanish Ministry of Science and Innovation (grant no. PID2021-124932OB-I00).

Appendix A. Supplementary data

Supplementary data to this article can be found online at https://doi.org/10.1016/j.jconrel.2025.114134.

Data availability

Data will be made available on request.

References

[1] F.J. Martinez, H.R. Collard, A. Pardo, G. Raghu, L. Richeldi, M. Selman, J. J. Swigris, H. Taniguchi, A.U. Wells, Idiopathic pulmonary fibrosis, Nat. Rev. Dis. Primers 3 (2017) 17074.
[2] R. Shah Gupta, A. Koteci, A. Morgan, P.M. George, J.K. Quint, Incidence and prevalence of interstitial lung diseases worldwide: a systematic literature review, BMJ Open Respir. Res. 10 (2023) e001291.
[3] N.N. Alrajhi, Post-COVID-19 pulmonary fibrosis: an ongoing concern, Ann. Thorac. Med. 18 (2023) 173–181.
[4] G. Raghu, D. Weycker, J. Edelsberg, W.Z. Bradford, G. Oster, Incidence and prevalence of idiopathic pulmonary fibrosis, Am. J. Respir. Crit. Care Med. 174 (2006) 810–816.
[5] J. Sauleda, B. Núñez, E. Sala, J.B. Soriano, Idiopathic pulmonary fibrosis: epidemiology, natural history, phenotypes, Med. Sci. 6 (2018) 110.
[6] F. Bonella, P. Spagnolo, C. Ryerson, Current and future treatment landscape for idiopathic pulmonary fibrosis, Drugs 83 (2023) 1581–1593.
[7] X. Bai, G. Zhao, Q. Chen, Z. Li, M. Gao, W. Ho, X. Xu, X.-Q. Zhang, Inhaled siRNA nanoparticles targeting IL11 inhibit lung fibrosis and improve pulmonary function post-bleomycin challenge, Sci. Adv. 8 (2022) eabn7162.
[8] L. Ding, S. Tang, W. Tang, D.D. Mosley, A. Yu, D. Sil, S. Romanova, K.L. Bailey, D. L. Knoell, T.A. Wyatt, D. Oupický, Perfluorocarbon Nanoemulsions enhance therapeutic siRNA delivery in the treatment of pulmonary fibrosis, Adv. Sci. 9 (2022) 2103676.
[9] Q. Wan, X. Zhang, D. Zhou, R. Xie, Y. Cai, K. Zhang, X. Sun, Inhaled nano-based therapeutics for pulmonary fibrosis: recent advances and future prospects, J. Nanobiotechnol. 21 (2023) 215.
[10] Y. Tang, X. Wang, J. Li, Y. Nie, G. Liao, Y. Yu, C. Li, Overcoming the reticuloendothelial system barrier to drug delivery with a "Don't-eat-us" strategy, ACS Nano 13 (2019) 13015–13026.
[11] M. Gao, J. Zhong, X. Liu, Y. Zhao, D. Zhu, X. Shi, X. Xu, Q. Zhou, W. Xuan, Y. Zhang, Y. Zhou, J. Cheng, Deciphering the role of PEGylation on the lipid nanoparticle-mediated mRNA delivery to the liver, ACS Nano 19 (2025) 5966–5978.
[12] H.M. Mansour, Y.S. Rhee, X. Wu, Nanomedicine in pulmonary delivery, Int. J. Nanomedicine 4 (2009) 299–319.
[13] M. Falahati, A. Hasan, H.A. Zeinabad, V. Serpooshan, J.H. von der Thüsen, T.L. M. ten Hagen, Engineering of pulmonary surfactant corona on inhaled nanoparticles to operate in the lung system, Nano Today 52 (2023) 101998.
[14] Z. Jin, Q. Gao, K. Wu, J. Ouyang, W. Guo, X.-J. Liang, Harnessing inhaled nanoparticles to overcome the pulmonary barrier for respiratory disease therapy, Adv. Drug Deliv. Rev. 202 (2023) 115111.
[15] C.A. Ruge, J. Kirch, C.-M. Lehr, Pulmonary drug delivery: from generating aerosols to overcoming biological barriers; therapeutic possibilities and technological challenges, Lancet Respir. Med. 1 (2013) 402–413.
[16] Y. Peng, Z.-N. Wang, A.-R. Xu, Z.-F. Fang, S.-Y. Chen, X.-T. Hou, Z.-Q. Zhou, H.-M. Lin, J.-X. Xie, X.X. Tang, D.-Y. Wang, N.-S. Zhong, Mucus hypersecretion and ciliary impairment in conducting airway contribute to alveolar mucus plugging in idiopathic pulmonary fibrosis, Front. Cell Dev. Biol. 9 (2022).
[17] S.K. Lai, Y.Y. Wang, J. Hanes, Mucus-penetrating nanoparticles for drug and gene delivery to mucosal tissues, Adv. Drug Deliv. Rev. 61 (2009) 158–171.
[18] Q. Hu, X. Bai, G. Hu, Y.Y. Zuo, Unveiling the molecular structure of pulmonary surfactant Corona on nanoparticles, ACS Nano 11 (2017) 6832–6842.
[19] C. Garcia-Mouton, A. Hidalgo, A. Cruz, J. Pérez-Gil, The Lord of the lungs: the essential role of pulmonary surfactant upon inhalation of nanoparticles, Eur. J. Pharm. Biopharm. 144 (2019) 230–243.
[20] S.S. Raesch, S. Tenzer, W. Storck, A. Rurainski, D. Selzer, C.A. Ruge, J. Perez-Gil, U.F. Schaefer, C.-M. Lehr, Proteomic and Lipidomic analysis of nanoparticle Corona upon contact with lung surfactant reveals differences in protein, but not lipid composition, ACS Nano 9 (2015) 11872–11885.

[21] G. Hu, B. Jiao, X. Shi, R.P. Valle, Q. Fan, Y.Y. Zuo, Physicochemical properties of nanoparticles regulate translocation across pulmonary surfactant monolayer and formation of lipoprotein Corona, ACS Nano 7 (2013) 10525–10533.
[22] S. Carregal-Romero, H. Groult, O. Cañadas, N.A. Gonzalez, A.V. Lechuga-Vieco, B. García-Fojeda, F. Herranz, J. Pellico, A. Hidalgo, C. Casals, J. Ruiz-Cabello, Delayed alveolar clearance of nanoparticles through control of coating composition and interaction with lung surfactant protein A, Biomater. Adv. 134 (2022) 112551.
[23] J. Li, H. Yang, S. Sha, J. Li, Z. Zhou, Y. Cao, Evaluation of in vitro toxicity of silica nanoparticles (NPs) to lung cells: influence of cell types and pulmonary surfactant component DPPC, Ecotoxicol. Environ. Saf. 186 (2019) 109770.
[24] Y. Gao, M. Joshi, Z. Zhao, S. Mitragotri, PEGylated therapeutics in the clinic, Bioeng. Transl. Med. 9 (2024) e10600.
[25] A.M. López-Estevez, R. Gref, M.J. Alonso, A journey through the history of PEGylated drug delivery nanocarriers, Drug Deliv. Transl. Res. 14 (2024) 2026–2031.
[26] A. Moreno, G.A. Pitoc, N.J. Ganson, J.M. Layzer, M.S. Hershfield, A.F. Tarantal, B. A. Sullenger, Anti-PEG antibodies inhibit the anticoagulant activity of PEGylated aptamers, Cell Chem. Biol. 26 (2019), 634-644.e633.
[27] R. Tenchov, J.M. Sasso, Q.A. Zhou, PEGylated lipid nanoparticle formulations: immunological safety and efficiency perspective, Bioconjug. Chem. 34 (2023) 941–960.
[28] Y. Ju, W.S. Lee, E.H. Pilkington, H.G. Kelly, S. Li, K.J. Selva, K.M. Wragg, K. Subbarao, T.H.O. Nguyen, L.C. Rowntree, L.F. Allen, K. Bond, D.A. Williamson, N.P. Truong, M. Plebanski, K. Kedzierska, S. Mahanty, A.W. Chung, F. Caruso, A. K. Wheatley, J.A. Juno, S.J. Kent, Anti-PEG antibodies boosted in humans by SARS-CoV-2 lipid nanoparticle mRNA vaccine, ACS Nano 16 (2022) 11769–11780.
[29] B.-M. Chen, T.-L. Cheng, S.R. Roffler, Polyethylene glycol immunogenicity: theoretical, clinical, and practical aspects of anti-polyethylene glycol antibodies, ACS Nano 15 (2021) 14022–14048.
[30] E. Blanco, H. Shen, M. Ferrari, Principles of nanoparticle design for overcoming biological barriers to drug delivery, Nat. Biotechnol. 33 (2015) 941–951.
[31] M.J. Guichard, T. Leal, R. Vanbever, PEGylation, an approach for improving the pulmonary delivery of biopharmaceuticals, Curr. Opin. Colloid Interface Sci. 31 (2017) 43–50.
[32] H. Zhang, Thin-film hydration followed by extrusion method for liposome preparation, Methods Mol. Biol. 1522 (2017) 17–22.
[33] J. Pellico, J. Ruiz-Cabello, I. Fernández-Barahona, L. Gutiérrez, A.V. Lechuga-Vieco, J.A. Enríquez, M.P. Morales, F. Herranz, One-step fast synthesis of nanoparticles for MRI: coating chemistry as the key variable determining positive or negative contrast, Langmuir 33 (2017) 10239–10247.
[34] V.K. Parmar, S.B. Desai, T. Vaja, RP-HPLC and UV spectrophotometric methods for estimation of Pirfenidone in pharmaceutical formulations, Indian J. Pharm. Sci. 76 (2014) 225–229.
[35] G. Rouser, A.N. Siakotos, S. Fleischer, Quantitative analysis of phospholipids by thin-layer chromatography and phosphorus analysis of spots, Lipids 1 (1966) 85–86.
[36] J. Lu, Y. Xu, J. Chen, F. Huang, Effect of lysophosphatidylcholine on behavior and structure of phosphatidylcholine liposomes, Sci. China Ser. C.-Life Sci. 40 (1997) 622–629.
[37] A.M. Smondyrev, M.L. Berkowitz, Structure of Dipalmitoylphosphatidylcholine/cholesterol bilayer at low and high cholesterol concentrations: molecular dynamics simulation, Biophys. J. 77 (1999) 2075–2089.
[38] Q. Xu, L.M. Ensign, N.J. Boylan, A. Schön, X. Gong, J.-C. Yang, N.W. Lamb, S. Cai, T. Yu, E. Freire, J. Hanes, Impact of surface polyethylene glycol (PEG) density on biodegradable nanoparticle transport in mucus ex vivo and distribution in vivo, ACS Nano 9 (2015) 9217–9227.
[39] B.C. Huck, O. Hartwig, A. Biehl, K. Schwarzkopf, C. Wagner, B. Loretz, X. Murgia, C.-M. Lehr, Macro- and microrheological properties of mucus surrogates in comparison to native intestinal and pulmonary mucus, Biomacromolecules 20 (2019) 3504–3512.
[40] A. Aiyer, J. Manos, The use of artificial sputum media to enhance investigation and subsequent treatment of cystic fibrosis bacterial infections, Microorganisms 10 (2022) 1269.
[41] L. Bühler, M.D. Enderle, N. Kahn, M. Polke, M.A. Schneider, C.P. Heußel, F.J. F. Herth, W. Linzenbold, Establishment of a tissue-mimicking surrogate for pulmonary lesions to improve the development of RFA instruments and algorithms, Biomedicines 10 (2022) 1100.
[42] E. Da Silva, C. Autilio, K.S. Hougaard, A. Baun, A. Cruz, J. Perez-Gil, J.B. Sørli, Molecular and biophysical basis for the disruption of lung surfactant function by chemicals, Biochim. Biophys. Acta Biomembr. 1863 (2021) 183499.
[43] S. Schürch, H. Bachofen, F. Possmayer, Surface activity in situ, in vivo, and in the captive bubble surfactometer, Comp. Biochem. Physiol. A Mol. Integr. Physiol. 129 (2001) 195–207.
[44] Y. Xu, O. Cañadas, A. Alonso, H. Franzyk, A. Thakur, J. Pérez-Gil, C. Foged, Effect of lipid-polymer hybrid nanoparticles on the biophysical function and lateral structure of pulmonary surfactant: mechanistic in vitro studies, J. Colloid Interface Sci. 654 (2024) 1111–1123.
[45] E. Conte, E. Gili, E. Fagone, M. Fruciano, M. Iemmolo, C. Vancheri, Effect of pirfenidone on proliferation, TGF-β-induced myofibroblast differentiation and fibrogenic activity of primary human lung fibroblasts, Eur. J. Pharm. Sci. 58 (2014) 13–19.
[46] A.V. Shinde, C. Humeres, N.G. Frangogiannis, The role of α-smooth muscle actin in fibroblast-mediated matrix contraction and remodeling, BBA-Mol. Basis Dis. 1863 (2017) 298–309.
[47] A.C. Anselmo, S. Mitragotri, Nanoparticles in the clinic: an update, Bioeng. Transl. Med. 4 (2019) e10143.
[48] L. Sercombe, T. Veerati, F. Moheimani, S.Y. Wu, A.K. Sood, S. Hua, Advances and challenges of liposome assisted drug delivery, Front. Pharmacol. 6 (2015).
[49] L. Rao, P. Zhu, M. Guo, M. Hu, X. Guo, Y. Du, G. Xu, Nebulized inhalation of nintedanib-loaded biomimetic nano-liposomes attenuated bleomycin-induced interstitial lung fibrosis in mice, Nano Today 56 (2024) 102298.
[50] D. Li, A. Zhao, J. Zhu, C. Wang, J. Shen, Z. Zheng, F. Pan, Z. Liu, Q. Chen, Y. Yang, Inhaled lipid nanoparticles alleviate established pulmonary fibrosis, Small 19 (2023) e2300545.
[51] C.J. Van Echteld, B. De Kruijff, J.G. Mandersloot, J. De Gier, Effects of lysophosphatidylcholines on phosphatidylcholine and phosphatidylcholine/cholesterol liposome systems as revealed by 31P-NMR, electron microscopy and permeability studies, Biochim. Biophys. Acta 649 (1981) 211–220.
[52] P. Gangurde, M. Mahmoudzadeh, Z. Gounani, A. Koivuniemi, P. Laurén, T. Lajunen, T. Laaksonen, Development of robust cationic light-activated thermosensitive liposomes: choosing the right lipids, Mol. Pharm. 20 (2023) 5728–5738.
[53] M. Berger, M. Degey, J. Leblond Chain, E. Maquoi, B. Evrard, A. Lechanteur, G. Piel, Effect of PEG anchor and serum on lipid nanoparticles: development of a nanoparticles tracking method, Pharmaceutics 15 (2023).
[54] W. Zhang, Z. Wang, C. Wu, Y. Jin, X. Liu, Z. Wu, J. Liu, The effect of DSPE-PEG (2000), cholesterol and drug incorporated in bilayer on the formation of discoidal micelles, Eur. J. Pharm. Sci. 125 (2018) 74–85.
[55] M. Regenold, P. Bannigan, J.C. Evans, A. Waspe, M.J. Temple, C. Allen, Turning down the heat: the case for mild hyperthermia and thermosensitive liposomes, Nanomedicine 40 (2022) 102484.
[56] Y. Dou, K. Hynynen, C. Allen, To heat or not to heat: challenges with clinical translation of thermosensitive liposomes, J. Control. Release 249 (2017) 63–73.
[57] A.S. Nosova, O.O. Koloskova, A.A. Nikonova, V.A. Simonova, V.V. Smirnov, D. Kudlay, M.R. Khaitov, Diversity of PEGylation methods of liposomes and their influence on RNA delivery, Medchemcomm 10 (2019) 369–377.
[58] H. Meng, Y. Xu, Pirfenidone-loaded liposomes for lung targeting: preparation and in vitro/in vivo evaluation, Drug Des. Devel. Ther. 9 (2015) 3369–3376.
[59] V. Parvathaneni, N.S. Kulkarni, S.K. Shukla, P.T. Farrales, N.K. Kunda, A. Muth, V. Gupta, Systematic development and optimization of inhalable Pirfenidone liposomes for non-small cell lung cancer treatment, Pharmaceutics 12 (2020).
[60] N.S. Vrandečić, M. Erceg, M. Jakić, I. Klarić, Kinetic analysis of thermal degradation of poly(ethylene glycol) and poly(ethylene oxide)s of different molecular weight, Thermochim. Acta 498 (2010) 71–80.
[61] A. Vila, H. Gill, O. McCallion, M.J. Alonso, Transport of PLA-PEG particles across the nasal mucosa: effect of particle size and PEG coating density, J. Control. Release 98 (2004) 231–244.
[62] Q. Liu, J. Xue, X. Zhang, J. Chai, L. Qin, J. Guan, X. Zhang, S. Mao, The influence of a biomimetic pulmonary surfactant modification on the in vivo fate of nanoparticles in the lung, Acta Biomater. 147 (2022) 391–402.
[63] X. Murgia, B. Loretz, O. Hartwig, M. Hittinger, C.-M. Lehr, The role of mucus on drug transport and its potential to affect therapeutic outcomes, Adv. Drug Deliv. Rev. 124 (2018) 82–97.
[64] A. Hidalgo, A. Cruz, J. Pérez-Gil, Barrier or carrier? Pulmonary surfactant and drug delivery, Eur. J. Pharm. Biopharm. 95 (2015) 117–127.
[65] B. Huck, A. Hidalgo, F. Waldow, D. Schwudke, K.I. Gaede, C. Feldmann, P. Carius, C. Autilio, J. Pérez-Gil, K. Schwarzkopf, X. Murgia, B. Loretz, C.-M. Lehr, Systematic analysis of composition, interfacial performance and effects of pulmonary surfactant preparations on cellular uptake and cytotoxicity of aerosolized nanomaterials, Small Sci. 1 (2021) 2100067.
[66] L. Fernández-Méndez, Y. Fernández-Afonso, P. Martínez-Vicente, A. Urkola-Arsuaga, C. Miranda-Pérez de Alejo, I.L. de la Pisa, S. Plaza-García, J. Ruíz-Cabello, P. Ramos-Cabrer, L. Gutiérrez, S. Carregal-Romero, NIR-II Photoresponsive Magnetoliposomes for remote-controlled release and magnetic resonance imaging, ACS Appl. Bio Mater. 8 (2025) 4855–4869.
[67] R. Guagliardo, J. Pérez-Gil, S. De Smedt, K. Raemdonck, Pulmonary surfactant and drug delivery: focusing on the role of surfactant proteins, J. Control. Release 291 (2018) 116–126.
[68] C. Casals, E. Miguel, J. Perez-Gil, Tryptophan fluorescence study on the interaction of pulmonary surfactant protein a with phospholipid vesicles, Biochem. J. 296 (Pt 3) (1993) 585–593.
[69] C.A. Ruge, H. Hillaireau, N. Grabowski, M. Beck-Broichsitter, O. Cañadas, N. Tsapis, C. Casals, J. Nicolas, E. Fattal, Pulmonary surfactant protein A-mediated enrichment of surface-decorated polymeric nanoparticles in alveolar macrophages, Mol. Pharm. 13 (2016) 4168–4178.
[70] N. Palaniyar, R.A. Ridsdale, C.E. Holterman, K. Inchley, F. Possmayer, G. Harauz, Structural changes of surfactant protein a induced by cations reorient the protein on lipid bilayers, J. Struct. Biol. 122 (1998) 297–310.
[71] Y. Kuroki, T. Akino, Pulmonary surfactant protein A (SP-A) specifically binds dipalmitoylphosphatidylcholine, J. Biol. Chem. 266 (1991) 3068–3073.
[72] J.Y. Liu, C.M. Sayes, Lung surfactant as a biophysical assay for inhalation toxicology, Curr. Res. Toxicol. 4 (2023) 100101.
[73] Y. Xu, E. Parra-Ortiz, F. Wan, O. Cañadas, B. Garcia-Alvarez, A. Thakur, H. Franzyk, J. Pérez-Gil, M. Malmsten, C. Foged, Insights into the mechanisms of interaction between inhalable lipid-polymer hybrid nanoparticles and pulmonary surfactant, J. Colloid Interface Sci. 633 (2023) 511–525.
[74] C.A. Ruge, U.F. Schaefer, J. Herrmann, J. Kirch, O. Cañadas, M. Echaide, J. Pérez-Gil, C. Casals, R. Müller, C.M. Lehr, The interplay of lung surfactant proteins and lipids assimilates the macrophage clearance of nanoparticles, PLoS One 7 (2012) e40775.

[75] J. Wang, P. Li, Y. Yu, Y. Fu, H. Jiang, M. Lu, Z. Sun, S. Jiang, L. Lu, M.X. Wu, Pulmonary surfactant–biomimetic nanoparticles potentiate heterosubtypic influenza immunity, Science 367 (2020) eaau0810.
[76] A. Gonsalves, P. Sorkhdini, J. Bazinet, M. Ghumman, D. Dhamecha, Y. Zhou, J. U. Menon, Development and characterization of lung surfactant-coated polymer nanoparticles for pulmonary drug delivery, Biomater. Adv. 150 (2023) 213430.
[77] J. Zhao, L. Qin, R. Song, J. Su, Y. Yuan, X. Zhang, S. Mao, Elucidating inhaled liposome surface charge on its interaction with biological barriers in the lung, Eur. J. Pharm. Biopharm. 172 (2022) 101–111.
[78] N. Roldan, Thomas K.M. Nyholm, J.P. Slotte, J. Pérez-Gil, B. García-Álvarez, Effect of lung surfactant protein SP-C and SP-C-promoted membrane fragmentation on cholesterol dynamics, Biophys. J. 111 (2016) 1703–1713.
[79] S. Chono, R. Fukuchi, T. Seki, K. Morimoto, Aerosolized liposomes with dipalmitoyl phosphatidylcholine enhance pulmonary insulin delivery, J. Control. Release 137 (2009) 104–109.
[80] B. Wang, Y. Gao, L. Sun, M. Xue, M. Wang, Z. Zhang, L. Zhang, H. Zhang, Inhaled pulmonary surfactant biomimetic liposomes for reversing idiopathic pulmonary fibrosis through synergistic therapeutic strategy, Biomaterials 303 (2023) 122404.
[81] D. Pozzi, V. Colapicchioni, G. Caracciolo, S. Piovesana, A.L. Capriotti, S. Palchetti, S. De Grossi, A. Riccioli, H. Amenitsch, A. Laganà, Effect of polyethyleneglycol (PEG) chain length on the bio–nano-interactions between PEGylated lipid nanoparticles and biological fluids: from nanostructure to uptake in cancer cells, Nanoscale 6 (2014) 2782–2792.
[82] M. Radiom, M. Sarkis, O. Brookes, E.K. Oikonomou, A. Baeza-Squiban, J.F. Berret, Pulmonary surfactant inhibition of nanoparticle uptake by alveolar epithelial cells, Sci. Rep. 10 (2020) 19436.
[83] S. Subramaniam, P. Joyce, L. Donnellan, C. Young, A. Wignall, P. Hoffmann, C. A. Prestidge, Protein adsorption determines pulmonary cell uptake of lipid-based nanoparticles, J. Colloid Interface Sci. 641 (2023) 36–47.
[84] X. Bai, M. Xu, S. Liu, G. Hu, Computational investigations of the interaction between the cell membrane and nanoparticles coated with a pulmonary surfactant, ACS Appl. Mater. Interfaces 10 (2018) 20368–20376.
[85] A. Hidalgo, A. Cruz, J. Pérez-Gil, Pulmonary surfactant and nanocarriers: toxicity versus combined nanomedical applications, Biochim. Biophys. Acta Biomembr. 1859 (2017) 1740–1748.
[86] Q. Fan, Y.E. Wang, X. Zhao, J.S.C. Loo, Y.Y. Zuo, Adverse biophysical effects of hydroxyapatite nanoparticles on natural pulmonary surfactant, ACS Nano 5 (2011) 6410–6416.
[87] N. Milad, M.C. Morissette, Revisiting the role of pulmonary surfactant in chronic inflammatory lung diseases and environmental exposure, Eur. Respir. J. 30 (2021) 210077.
[88] C.J. Scotton, R.C. Chambers, Molecular targets in pulmonary fibrosis: the Myofibroblast in focus, Chest 132 (2007) 1311–1321.
[89] M. Liu, Q. Li, L. Liang, J. Li, K. Wang, J. Li, M. Lv, N. Chen, H. Song, J. Lee, J. Shi, L. Wang, R. Lal, C. Fan, Real-time visualization of clustering and intracellular transport of gold nanoparticles by correlative imaging, Nat. Commun. 8 (2017) 15646.
[90] M.J. Song, S.W. Moon, J.S. Choi, S.H. Lee, S.H. Lee, K.S. Chung, J.Y. Jung, Y. A. Kang, M.S. Park, Y.S. Kim, J. Chang, S.Y. Kim, Efficacy of low dose pirfenidone in idiopathic pulmonary fibrosis: real world experience from a tertiary university hospital, Sci. Rep. 10 (2020) 21218.
[91] C.A. Ruge, J. Kirch, C.-M. Lehr, Pulmonary drug delivery: from generating aerosols to overcoming biological barriers—therapeutic possibilities and technological challenges, Lancet Respir. Med. 1 (2013) 402–413.
[92] Y. Morimoto, H. Izumi, Y. Yoshiura, K. Fujishima, K. Yatera, K. Yamamoto, Usefulness of intratracheal instillation studies for estimating nanoparticle-induced pulmonary toxicity, Int. J. Mol. Sci. 17 (2016) 165.
[93] G. Oberdörster, C. C, R. Gelein, Intratracheal instillation versus Intratracheal inhalation of tracer particles for measuring lung clearance function, Exp. Lung Res. 23 (1997) 17–34.
[94] L. Wu, C. Rodríguez-Rodríguez, D. Cun, M. Yang, K. Saatchi, U.O. Häfeli, Quantitative comparison of three widely-used pulmonary administration methods in vivo with radiolabeled inhalable nanoparticles, Eur. J. Pharm. Biopharm. 152 (2020) 108–115.
[95] N. Tanabe, J.E. McDonough, D.M. Vasilescu, K. Ikezoe, S.E. Verleden, F. Xu, W. A. Wuyts, B.M. Vanaudenaerde, T.V. Colby, J.C. Hogg, Pathology of idiopathic pulmonary fibrosis assessed by a combination of microcomputed tomography, histology, and immunohistochemistry, Am. J. Pathol. 190 (2020) 2427–2435.
[96] K. Togami, Y. Maruta, M. Nanbu, H. Tada, S. Chono, Prolonged distribution of aerosolized PEGylated liposomes in the lungs of mice with bleomycin-induced pulmonary fibrosis, Drug Dev. Ind. Pharm. 46 (2020) 1873–1880.
[97] M. Jang, K. Yeom, J. Han, E. Fagan, J.-H. Park, Inhalable mRNA nanoparticle with enhanced nebulization stability and pulmonary microenvironment infiltration, ACS Nano 18 (2024) 24204–24218.
[98] M.P. Lokugamage, D. Vanover, J. Beyersdorf, M.Z.C. Hatit, L. Rotolo, E. S. Echeverri, H.E. Peck, H. Ni, J.-K. Yoon, Y. Kim, P.J. Santangelo, J.E. Dahlman, Optimization of lipid nanoparticles for the delivery of nebulized therapeutic mRNA to the lungs, Nat. Biomed. Eng. 5 (2021) 1059–1068.
[99] J. Kim, A. Jozić, E. Bloom, B. Jones, M. Marra, N.T.V. Murthy, Y. Eygeris, G. Sahay, Microfluidic platform enables Shearless Aerosolization of lipid nanoparticles for mRNA inhalation, ACS Nano 18 (2024) 11335–11348.
[100] S. Liu, Y. Wen, X. Shan, X. Ma, C. Yang, X. Cheng, Y. Zhao, J. Li, S. Mi, H. Huo, W. Li, Z. Jiang, Y. Li, J. Lin, L. Miao, X. Lu, Charge-assisted stabilization of lipid nanoparticles enables inhaled mRNA delivery for mucosal vaccination, Nat. Commun. 15 (2024) 9471.
[101] M. Röhrich, D. Leitz, F.M. Glatting, A.K. Wefers, O. Weinheimer, P. Flechsig, N. Kahn, M.A. Mall, F.L. Giesel, C. Kratochwil, P.E. Huber, A.v. Deimling, C. P. Heußel, H.U. Kauczor, M. Kreuter, U. Haberkorn, Fibroblast activation protein–Specific PET/CT imaging in fibrotic interstitial lung diseases and lung cancer: a translational exploratory study, J. Nucl. Med. 63 (2022) 127–133.
[102] G. Villetti, Y. Ridwan, S. Belenkov, J. Essers, F. Ruscitti, F. Ravenetti, P. Van Heiningen, W. Wos, C. Van Holsbeke, M. Civelli, F. Stellari, Longitudinal assessment of lung fibrosis by micro CT correlates with histological evaluation in bleomycin-induced mice, n.d. Eur. Clin. Respir. J., 48 OA3505.
[103] R. Trivedi, E.F. Redente, A. Thakur, D.W.H. Riches, U.B. Kompella, Local delivery of biodegradable pirfenidone nanoparticles ameliorates bleomycin-induced pulmonary fibrosis in mice, Nanotechnology 23 (2012) 505101.